Quaternary Science Reviews 76 (2013) 1–15

Contents lists available at SciVerse ScienceDirect

Quaternary Science Reviews

journal homepage: www.elsevier.com/locate/quascirev

Invited review

Latest Pleistocene to Holocene hydroclimates from Lake Elsinore, California

Matthew E. Kirby [a,*], Sarah J. Feakins [b,*], Nicole Bonuso [a], Joanna M. Fantozzi [a], Christine A. Hiner [a]

[a] California State University, Fullerton, Department of Geological Sciences, Fullerton, CA 92834, USA
[b] University of Southern California, Department of Earth Sciences, Los Angeles, CA 90089, USA

ARTICLE INFO

Article history:
Received 1 October 2012
Received in revised form
19 May 2013
Accepted 22 May 2013
Available online 26 June 2013

Keywords:
Deglacial
Southwest United States
Dipping westerlies
Hydrogen isotope
Lake Elsinore

ABSTRACT

The hydroclimate of the southwestern United States (US) region changed abruptly during the latest Pleistocene as the continental ice sheets over North America retreated from their most southerly extent. To investigate the nature of this change, we present a new record from Lake Elsinore, located 36 km inland from the Pacific Ocean in Southern California and evaluate it in the context of records across the coastal and interior southwest United States, including northwest Mexico. The sediment core recovered from Lake Elsinore provides a continuous sequence with multi-decadal resolution spanning 19–9 ka BP. Sedimentological and geochemical analyses reveal hydrologic variability. In particular, sand and carbonate components indicate abrupt changes at the Oldest Dryas (OD), Bølling–Allerød (BA), and Younger Dryas (YD) transitions, consistent with the timing in Greenland. Hydrogen isotope analyses of the C_{28} *n*-alkanoic acids from plant leaf waxes (δD_{wax}) reveal a long term trend toward less negative values across 19–9 ka BP. δD_{wax} values during the OD suggest a North Pacific moisture source for precipitation, consistent with the dipping westerlies hypothesis. We find no isotopic evidence for the North American Monsoon reaching as far west as Lake Elsinore; therefore, we infer that wet/dry changes in the coastal southwest were expressed through winter-season precipitation, consistent with modern climatology. Comparing Lake Elsinore to other southwest records (notably Cave of Bells and Fort Stanton) we find coincident timing of the major transitions (OD to BA, BA to YD) and hydrologic responses during the OD and BA. The hydrologic response, however, varied during the YD consistent with a dipole between the coastal and interior southwest. The coherent pattern of hydrologic responses across the interior southwest US and northwest Mexico during the OD (wet), the BA (drier), and YD (wet) follows changes in the Atlantic Meridional Overturning Circulation, presumably via its combined influence on North Pacific winter storm tracks and the extent/magnitude of the North American Monsoon. In contrast, Lake Elsinore and the coastal southwest experiences a deglacial drying trend punctuated by abrupt change at the OD to BA and BA to YD transitions. This trend tracks rising greenhouse gases through the deglacial, with an apparent southward shift in westerly moisture sources adjusting to the retreating ice sheet.

1. Introduction

The rates and amplitude of climatic change associated with global warming over the next century are expected to extend beyond that recorded by instrumental records (IPCC, 2007). Abrupt climatic transitions that cause permanent shifts in regional mean climatic states are of particular concern (Overpeck, 1996). Climate model projections for the southwest United States predict a change in the frequency and magnitude of precipitation, perhaps with an overall drying (Beuhler, 2003; Seager et al., 2007; Dominguez et al., 2012). Any change to the region's hydroclimatology likely will have costly consequences for the highly populous, water-stressed region (e.g., Smith, 2011). Here we seek evidence for past hydroclimatic change and offer insights into spatial differences within the southwest that may be key for projecting how these systems respond in the future. For the water-stressed southwest, there is a particular urgency to understand the causes and spatial patterns of hydrologic change, particularly abrupt changes (Seager et al., 2005; Cook et al., 2011). The most recent glacial termination at the end of the Pleistocene and start of the Holocene (hereafter most recent deglacial) provides evidence for large amplitude variability

* Corresponding authors.
E-mail addresses: mkirby@fullerton.edu (M.E. Kirby), feakins@usc.edu (S.J. Feakins).

0277-3791/$ – see front matter © 2013 Elsevier Ltd. All rights reserved.
http://dx.doi.org/10.1016/j.quascirev.2013.05.023

punctuated by rapid transitions between climatic states (e.g., Clark et al., 2012). Here, we explore the implications for the hydroclimates of the southwest United States and northwest Mexico during the most recent glacial termination.

Evaluation of terrestrial climate for the region was limited previously by the lack of a high resolution, complete deglacial sequence from the coastal southwest. In the absence of a coastal southwest terrestrial site, marine archives were used to infer terrestrial climate change during the most recent deglacial (Lyle et al., 2010, 2012). We present a new record from Lake Elsinore, California, which fills this geographic gap in the coastal southwest. We analyze climatic transitions across the region primarily through comparison to the interior southwest records from Cave of Bells, Arizona (Wagner et al., 2010) and Fort Stanton, New Mexico (Asmerom et al., 2010). Eight additional sites add to the millennial-scale evidence for hydroclimatic change across the region; although, their contributions are limited variously by lower temporal resolution of sampling and age control. The objective of the regional comparison is to identify the spatial patterns of hydrologic change across the study area during the most recent deglacial. We explore further the drivers of most recent deglacial through the principal "modes of deglacial variability" identified by Clark et al. (2012). Specifically we seek to test which of the two principal modes – radiative or Atlantic Meridional Overturning Circulation (AMOC) forcings (Clark et al., 2012) – dominate the response in the coastal (Lake Elsinore) and interior (Cave of Bells and Fort Stanton) southwest. Lastly we use insights from compound specific hydrogen isotopic measurements at Lake Elsinore to evaluate the 'dipping westerlies' hypothesis. This hypothesis states that during the most recent glacial the dominant westerly storm track that transported precipitation to the west coast of the United States, was redirected further south in response to the position of the North American ice sheets (Negrini, 2002; cf. Lyle et al., 2010, 2012).

1.1. Regional climatology

Across the coastal and interior southwest US and northern Mexico (Fig. 1), the seasonality of precipitation varies between Mediterranean, desert, and monsoon regimes (Comrie and Glenn, 1998). Wet winters and dry summers characterize the Mediterranean precipitation regime. The desert precipitation regime is annually dry with small winter and late-summer precipitation contributions; whereas, the monsoon precipitation regime is dominated by late-summer to early fall precipitation maxima with a small winter contribution. Two meteorological sites (Ensenada, Mexico; and, Phoenix, Arizona) fall within the transitional precipitation regime; no sites fall within the Texas/Oklahoma regime (eastern edge of Fig. 1).

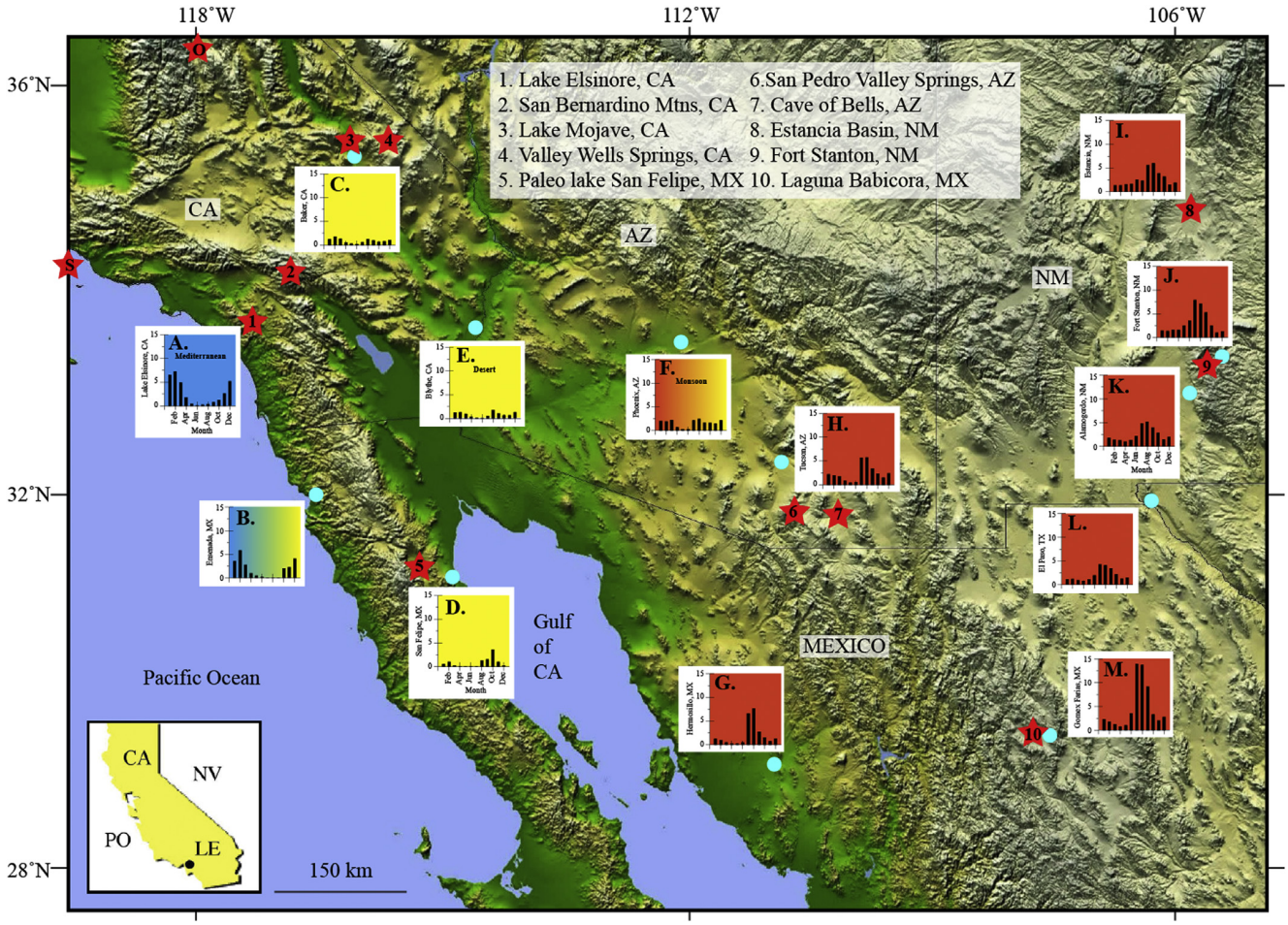

Fig. 1. Regional map with study sites and precipitation regimes. Blue = Mediterranean climate; Yellow = Desert climate; Orange = Monsoon climate. Red stars with numbers represent study site locations. Light blue dots represent precipitation sites. If the study site and the precipitation sites are the same (e.g., Lake Elsinore), the red star is only shown. S = Santa Barbara Basin. O = Owens Lake. Precipitation data from www.weatherbase.com and/or http://www.ncdc.noaa.gov.

The winter-season precipitation is almost exclusively derived from Pacific Ocean moisture sources (Friedman et al., 1992, 2002a; Ely et al., 1994; Williams and Rodoni, 1997). The amount of winter precipitation is determined by the position of the winter polar front, modulated by changes in the location of the eastern Pacific subtropical high (Cayan and Peterson, 1989; Burnett, 1994; Ely et al., 1994). A strong high-pressure ridge off the west coast steers Pacific storms northward and causes dry winters in the southwest. Conversely, wet southwest winters are caused by a weakening of the subtropical high, with a southward shift in the westerlies and an increase in the potential for atmospheric rivers and associated heavy precipitation (Ely et al., 1994; Neiman et al., 2008; Dettinger et al., 2011; Kirby et al., 2012). Today, where there are only playas, many paleo-lakes indicate that precipitation in the region was enhanced during the Last Glacial (e.g., Allen and Anderson, 2000; Negrini, 2002; Tchakerian and Lancaster, 2002). Many climate models similarly predict higher precipitation during the most recent glacial (Bartlein et al., 1998; Kim et al., 2008; Unterman et al., 2011). Enhanced winter precipitation is generally attributed to a southward-displaced winter season polar front (dipping westerlies) (e.g., Negrini, 2002); although, an alternative hypothesis implicates subtropical moisture sources including a stronger North American Monsoon (NAM; Lyle et al., 2010, 2012).

NAM brings precipitation to the southwestern United States between late-summer and early fall. Moisture sources include the Gulf of California and the Gulf of Mexico (Adams and Comrie, 1997; Sheppard et al., 2002). The amount of moisture advected by the NAM is controlled by Gulf of CA and Mexico sea surface temperatures, easterly wave activity, and the position of the Gulf of Mexico high pressure system (Stensrud et al., 1995; Adams and Comrie, 1997). In addition, dissipating eastern Pacific tropical cyclones may reach the southwest (Ritchie et al., 2011). Although less frequent than monsoonal storms, tropical cyclones can generate a large amount of precipitation in a short period of time and, spatially, they can impact all parts of the study area including, rarely, the winter precipitation dominated coastal southwest United States. Later in the cyclone season, as mid-latitude Pacific troughs migrate southward the opportunity for mid-latitude waves to entrain tropical cyclones increases (Lawrence et al., 2001).

Each of these moisture sources has distinct isotopic compositions, which can be used to differentiate the dynamical causes of wet and dry shifts. Isotopic differences arise largely from the different rainout histories of the various storm tracks and show the greatest distinction between northwesterly sources from the North Pacific (more negative) and southerly sources from the subtropical and tropical Pacific, Gulfs of Mexico and California (less negative). Specific values are not given here as the values change along the storm track; however, the offset between northerly and southerly sources at Cedar City, Utah is between ~30 and 50‰ (Friedman et al., 2002a). In general, summer precipitation is characterized by higher δD values than winter due both to the higher temperatures of condensation as well as the more southerly sources of moisture (Friedman et al., 1992, 2002a, 2002b; Williams and Rodoni, 1997; Wright et al., 2001). Shifts in the predominance and source of winter westerly precipitation and summer southerly precipitation can therefore be examined using proxies that capture the isotopic composition of precipitation through time. The dipping westerlies of the most recent glacial would therefore be expected to be associated with more D-depleted precipitation relative to today.

1.2. The Playa lakes of the desert southwest

Playa lakes in the interior southwest US and northwest Mexico partially fill during only the most extreme winters today, and once full, they retain water only for a brief interval (months to years; Enzel and Wells, 1997). The high potential evaporation during summer in the interior southwest US and northwest Mexico means that monsoonal precipitation cannot sustain lakes in the region, and summer precipitation generally has a negligible impact on the region's annual hydrologic budget (Sheppard et al., 2002). Instead, it is winter precipitation that matters to the region's annual hydrologic budget. Today, winter precipitation is too scarce to sustain lakes in the interior southwest US and northwest Mexico. However, closer to the coast and downstream of orographic barriers such as the Transverse and Peninsular Ranges of the coastal southwest US (with elevations of ~3 km), precipitation amounts are sufficient to sustain lakes such as Lake Elsinore with only rare, short-lived intervals of pre-historic desiccation (Kirby et al., 2004). Based on this modern gradient in the amount of winter precipitation across the study region, Lake Elsinore is uniquely positioned to capture changes in the intensity of the winter moisture flux (Kirby et al., 2010). Any change to Lake Elsinore's hydrologic budget reflects a change in the amount of winter precipitation without the added complexity of monsoonal moisture felt further inland. For the interior southwest US and northwest Mexico, we contend that winter, too, will matter most to the region's hydrology, although, lower potential evaporation during the most recent glacial could make monsoonal moisture more important than at present to the hydrologic budget. Within the Mediterranean precipitation regime Lake Elsinore provides a unique opportunity to deconvolve the seasonality of moisture during the latest Pleistocene across a large region characterized by two distinct precipitation regimes. As it is distinctly winter dominated, Lake Elsinore is also well positioned to capture changes in the source of winter season precipitation (e.g., North Pacific versus subtropical and tropical Pacific).

1.3. Lake Elsinore

Lake Elsinore is located (~377 m asl) at the base of the Santa Ana Mountains (locally the Elsinore Mountains), 36 km inland from the Pacific Ocean in Southern California (Fig. 2). The lake is in a pull-apart basin formed by fault step-over from the Glen Ivy North Fault to the Wildomar Fault (Hull, 1990). Fault slip rate estimates suggest that the horizontal to vertical slip ratio is in excess of 10:1 over the past ~2.5 Myr (Hull and Nicholson, 1992). Faulting is unlikely to account for more than 1–2 m of fault-generated lake level change; whereas, hydrologic change of up to 13 m has been noted in the historical record (Vaughan et al., 1999). As an additional test for seismic disturbance of lake sediments we used chirp and boomer seismic reflection data (Pyke et al., 2009). Pyke's study found no visible evidence for seismic disturbance and instead found continuous sedimentation through the upper 20 m of sediments in the lake's depocenter. Strong signal attenuation prevented deeper seismic imaging.

The lake occupies a maximum modern surface area of approximately 2.5 km wide by 11 km long, making it the largest, natural permanent lake in Southern California (Kirby et al., 2004). The surface area of the lake fluctuates significantly with interannual variations in precipitation (Kirby et al., 2010). Lake Elsinore is predominantly a closed-basin lake; however, historical records indicate that the lake has overflowed at least 20 times since 1769 AD (Lynch, 1931). The primary water source for the lake is the San Jacinto River, which drains approximately 1240 km^2, including parts of the San Jacinto Mountains in the Peninsular Range. Direct run-off from the nearby Elsinore Mountains is an additional local water source. Lake Elsinore is typically polymictic with a maximum modern depth of 13 m until spill-over (Anderson, 2001). Bottom water anoxia is common at Lake Elsinore in response to thermal stratification and intense primary productivity (Anderson, 2001). Evaporation accounts for >1.4 m of water loss per year, and $CaCO_3$

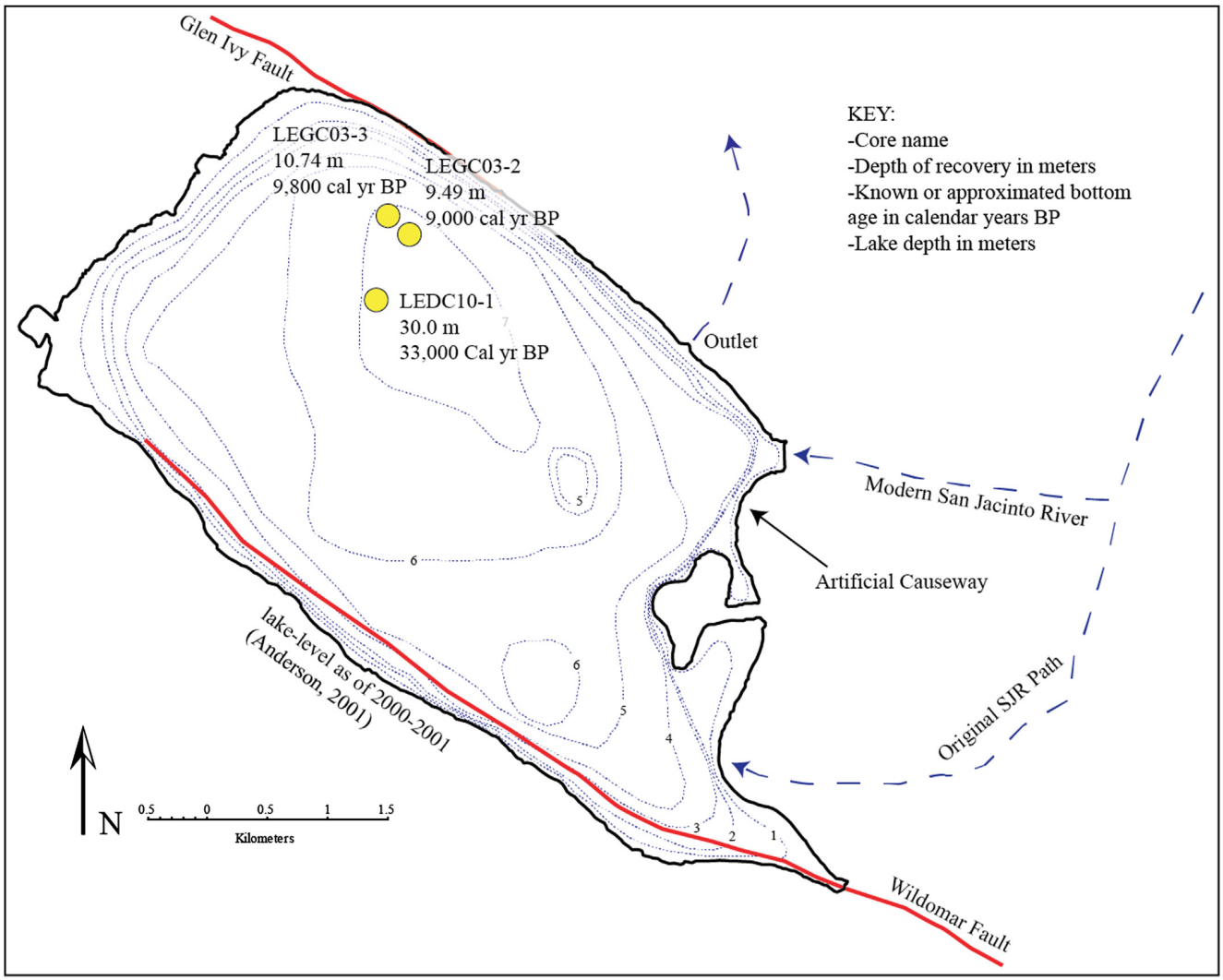

Fig. 2. Lake Elsinore bathymetry map using data from Anderson (2001). Core locations shown with basal age.

precipitates within the epilimnion likely in response to photosynthetic drawdown of CO_2 (Anderson, 2001).

2. Methods

2.1. Sediment coring and age model

Core LEDC10-1 was extracted over three days in June 2010 using a hollow stemmed auger push core system with a lined hole aboard a stabilized coring barge (Fig. 2). Each drive was 0.61 m and recovery was better than 90% for the total core length. Site selection was based on the location of the thickest sediment package according to the seismic reflection data (Pyke et al., 2009). Coring began 9 m below the modern sediment–water interface to provide some overlap with cores LEGC03-2 (9.49 m) and -3 (10.74 m) collected previously from the lake in 2003 using the same coring method (Fig. 2; Kirby et al., 2010). LOI data confirm the overlap between LEGC03-2 and -3 and LEDC10-1. Coring ended at 30 m below the sediment–water interface (due to budget limits; there are no physical impediments to deeper coring). The age model, stratigraphy and seismic reflection data indicate continuous sedimentation from 19 to 9 ka BP.

The core was split, digitally photographed, described, sampled, and stored at 4 °C at the CSUF Paleoclimatology and Paleotsunami Laboratory. Twenty-two samples (including three duplicates and three paired macrofossil and bulk samples) of either discrete organic material ($n = 15$) or bulk organic material ($n = 7$) were collected for AMS ^{14}C dating. All ^{14}C samples were treated with an acid wash to remove any carbonate and measured at the Lawrence Livermore National Laboratory's Center for Accelerator Mass Spectrometry (LLNL-CAMS).

2.2. Sedimentary analyses

Magnetic susceptibility values were measured at 1 cm contiguous intervals using a Bartington MS2 and MS2B magnetic susceptibility meter at 0.465 kHz. Samples were measured immediately after the core was sampled to minimize the possibility of mineral alteration through exposure to air. Results are reported in SI units ($\times 10^{-7}$ m^3 kg^{-1}).

Total organic matter content (at 550 °C) and total carbonate content (at 950 °C) were measured using the loss on ignition (LOI) procedure (Dean, 1974). Samples were extracted at 1.0 cm contiguous intervals. Total carbonate values lower than 3–4% are

interpreted to be zero since the mass lost may only be an artifact of clay dehydration (Dean, 1974).

Total nitrogen (N_{total}), total carbon (C_{total}), and total organic carbon content were determined at every other centimeter using a Costech 4010 Elemental Analyzer. Acidification of bulk sediments has been reported to change the nitrogen content in an unpredictable way (e.g., Brodie et al., 2011) and tests on the Elsinore sediment confirm the acidification effect (Fantozzi, 2011). Therefore, every sample was split and analyzed both untreated and acidified with 1 N HCl. The untreated sample split was analyzed for N_{total} and C_{total}. The acidified sample was used to determine total organic carbon content (C_{org}). C_{org}/N_{total} values (hereafter C:N) were calculated for each (following McFadden et al., 2005).

Grain size distribution was determined at every other centimeter. All grain size samples were treated with 30 mL 30% H_2O_2 to remove organic matter, 10–20 mL 1 N HCl to remove carbonates, and 10 mL NaOH to remove biogenic silica. Grain size was measured on a Malvern Mastersizer 2000 laser diffraction grain size analyzer coupled to a Hydro 2000G. To assess precision and accuracy, a tuff standard (TS2) with a known distribution between 1.0 and 16.0 μm (TS2 average = 4.56 ± 0.16 μm; $n = 5994$) was measured twice and compared to past measurements. Thereafter, TS2 was run every 10 samples to verify analytical repeatability and stability and at the end of the day. TS2 results are compared to values obtained by measuring known Malvern standards as an additional measure of stability. All data are reported as percent by volume and divided into 10 grain-size intervals.

2.3. Lipid extraction and isotopic analyses

Samples were collected for compound specific isotopic analyses across key transitions in the sand record, and sampling ~every 42 cm combining 2 cm of material. Sediments were freeze-dried and homogenized using a mortar and pestle, before solvent extraction with 9:1 dichloromethane (DCM) to methanol (MeOH) at 100 °C and 1500 psi using an Accelerated Solvent Extraction system (ASE 350®, Dionex). Total lipid extracts were separated by column chromatography over LC-NH_2 gel using 2:1 DCM:isopropanol (neutral fraction) and 4% formic acid in diethyl ether (acid fraction). The acid fraction was derivatized using MeOH of known isotopic composition in hydrochloric acid (70 °C for 12 h), before being diluted with milliQ H_2O and partitioned into hexane. The hexane fraction was further purified by column chromatography over silica gel (column: 5 cm × 4 mm Pasteur pipette, 5% water-deactivated silica-gel, 100–200 mesh) and eluted with hexane and DCM respectively. The DCM fraction containing the saturated fatty acid methyl esters (FAMEs) was evaporated under N_2 and dissolved in hexane for analysis.

FAMEs were analyzed by gas chromatography–mass spectrometry (GC–MS) to identify molecular composition and relative abundances (Agilent 6890 system, Rxi®-5ms, 30 m × 0.25 mm, film thickness 0.25 μm). δD values of *n*-alkane and *n*-alkanoic acid methyl ester fractions were analyzed at the University of Southern California (USC) using a Thermo Scientific Trace gas chromatograph connected via an Isolink parallel pyrolysis furnace (at 1400 °C) to a Delta V Plus mass spectrometer. The GC conditions included a ZB-5ms column (30 m × 0.25 mm × 1 μm) and a Programmable Temperature Vaporization (PTV) injector operated in solvent split mode. Peaks of hydrogen reference gas bracketed analyte peaks during the course of the GC–IRMS run. Two of the peaks were used for standardization of the isotopic analyses, while the others were treated as unknowns to assess accuracy. Data were then normalized to the VSMOW/SLAP isotopic scale by comparison with an external standard containing 8 fatty acid methyl esters (*i*-C_{14} to *i*-C_{20}; obtained from A. Schimmelmann, Indiana University, Bloomington) with δD values ranging from −167 to −231‰ (Sessions et al., 2001). The accuracy of replicate analyses of the external *n*-external standard was 4‰ (RMS error, $n = 21$). The results are reported using conventional delta notation (δD ‰).

2.4. Statistical analyses

We conducted multivariate statistical analysis to identify the dominant sedimentological components and sediment units, using Primer-E Ltd. software. We included measurements for magnetic susceptibility, LOI 550 °C, LOI 950 °C, C:N, clay, silt, and sand ($n = 261$) in the analysis. δD_{wax} data were not included because of their lower sampling resolution. Proxy data were standardized. We produced a resemblance matrix from the standardized dataset with respect to Euclidean distance. Samples were grouped using a hierarchical agglomerative clustering analysis. The Euclidean distance between cluster groups was calculated as the average similarity of the individual nodes within each group. From this data, we produced a cluster tree diagram (data not shown) to identify groupings. We performed a Principal Component Analysis (PCA) and coded each sample in correspondence to the main groupings determined by the cluster analysis (i.e., symbols on plot). Sample variables are superimposed on the scatter plot (i.e., radiating lines on plot) indicating the linear trend of each variable, or proxy, within the dataset. To test the significance of groupings, we performed the Analysis of Similarities (ANISOM) to quantitatively assess the uniqueness of the groups determined by the cluster analysis. The null hypothesis states that there are no differences between the cluster groups. If the value of the calculated test statistic, *R*, is close to zero (one), then the null hypothesis is true (false).

3. Results

3.1. Age control

22 AMS ^{14}C dates obtained from this core interval (Table 1). Paired discrete and bulk dates ($n = 3$) were measured at three depths to allow for the assessment and calculation of an old carbon effect; the bulk ages in these paired samples were not used in the age model. The average difference in age between the three paired discrete and bulk dates (915 ± 163 yrs; Table 2) was subtracted from every unpaired bulk date ($n = 4$) to obtain a "corrected" bulk age for the age model (Table 2, Fig. 3). An age model was constructed using a third order polynomial (Fig. 3). Radiocarbon years were calibrated and converted to calendar years before present using the CALIB 6.0.1 Program (Stuiver et al., 1998).

3.2. Sediment description

A ~6.5 m section of sediment from LEDC10-1 spanning approximately 19–9 ka BP is used for this study. This section is characterized by three distinct sediment types unrelated to the statistical units (Fig. 4). Type 1 (19.2–16.1 m) is dominated by a well-to-faintly laminated light to dark brown mud. Occasional visible, discrete organic matter in the form of very small woody pieces, seeds (?), and charcoal is present. Type 2 (16.1–15.2 m) is brown–green faintly laminated sediment overprinted by mottling that grades up-core to massive and mottled gray sediment. Type 3 is (15.2–12.6 m) is characterized as massive light to dark olive-gray mud. Type 3 is characterized by mottling throughout that varies in both color and intensity. Thin layers of broken gastropod shells at 14.18, 13.45, and 12.74 m are the only sources of visible, discrete organic matter within Type 3.

Table 1
Age data.

#	Depth range (cm)	Average depth (cm)	Material	LLNL AMS results				Calibration results[b]	
				ID	$\delta^{13}C$ (‰)[a]	^{14}C age (BP)	±	2-Sigma range	Age (cy BP)
1	1274–1275	1274.5	Gastropods	N93630	−25	8655	35	9541–9684	9613
2	1274–1275	1274.5	Gastropods	N93631	−25	8710	35	9548–9780	9664
3	1396–1398	1397.0	Bulk	94679	−25	10,155	45	11,685–12,030	11,858
4	1508–1510	1509.0	Bulk	94680	−22.9	10,950	40	12,648–12,964	12,806
5	1540–1542	1541.0	Bulk	94681	−25	11,650	60	13,334–13,691	13,513
6	1618–1620	1619.0	Bulk	94682	−24.6	12,200	35	13,887–14,202	14,045
7	1683–1685	1684.0	Mixed discrete	N95444	−25	12,140	280	13,437–15,067	14,252
8	1710–1711	1710.5	Mixed discrete	N95445	−25	12,460	120	14,091–15,090	14,591
9	1738–1739	1738.5	Mixed discrete	N95446	−25	13,420	230	15,390–16,932	16,161
10	1747–1748	1747.5	Bulk	N94683	−26.4	13,880	40	16,782–17,144	16,963
11	1747–1748	1747.5	Charcoal	N94003	−25	13,260	35	15,578–16,699	16,139
12	1778–1779	1778.5	Wood	N94004	−25	13,775	35	16,734–17,049	16,892
13	1823–1824	1823.5	Bulk	N94684	−25	15,250	60	18,466–18,688	18,577
14	1823–1824	1823.5	Charcoal	N94005	−25	14,360	30	17,154–17,790	17,472
15	1823–1824	1823.5	Charcoal	N94243	−25	14,310	30	17,082–17,706	17,394
16	1997–1999	1998.0	Seeds	N94006	−25	16,580	40	19,461–19,936	19,699
17	2019–2020	2019.5	Bulk	N94685	−22.5	17,490	70	20,447–21,257	20,852
18	2019–2020	2019.5	Seeds	N94007	−25	16,880	40	19,832–20,321	20,077
19	2081–2082	2081.5	Wood	N94008	−25	17,980	180	20,911–22,128	21,520
20	2198–2199	2198.5	Seeds	N94010	−25	19,630	40	23,134–23,779	23,457
21	2344–2345	2344.5	Charcoal	N94245	−25	21,025	40	24,940–25,556	25,248
22	2344–2345	2344.5	Charcoal	N94011	−25	21,120	70	24,834–25,494	25,164

[a] $\delta^{13}C$ values are the assumed values according to Stuiver et al. (1998) when given without decimal places. $\delta^{13}C$ values measured for the material itself are given with a single decimal place.
[b] CALIB 6.0.1 Program (Stuiver et al., 1998).

3.3. Proxy analyses

The magnetic susceptibility for the studied section in LEDC10-1 is variable (Fig. 4), although between 17.0 and 14.0 m, the amplitude of variability increases. Total organic matter values for the studied section range from 4.8 to 16.7% (Fig. 4). Organic matter increases slowly between 18.5 and 16.9 m but spikes to higher values between 18.1 and 17.9 m; values remain high and moderately variable until they steadily decrease between 15.7 and 15.0 m; from 15.0 to 12.6 m, the values are relatively low and stable. Total carbonate values range from 1.2 to 27.2% (Fig. 4). From 19.2 to 16.9 m, the values are uniformly low averaging 5.1%. Starting at 16.9 m, total carbonate values rise reaching ~18% by 16.6 m (Fig. 4). From 16.6 to 12.9 m, total carbonate values are generally high and variable. There are, however, two notable intervals of low carbonate values between 15.6–15.2 m and 13.0–12.6 m (Fig. 4). C:N values range from 4.3 to 15.3 with an average of 10.4 (Fig. 4). The values steadily increase between 18.5 and 16.6 m, with a sharp spike to higher values between 18.1 and 17.9 m. From 16.6 to 15.4 m, the C:N values are high and relatively stable. At 15.4 m up to 12.6 m, the C:N values are characterized by large amplitude and high frequency variability. The studied section of core LEDC10-1 is predominantly a clayey silt with generally <12% sand contribution (Fig. 4). Percent silt varies about its mean value with no demonstrable trends. Clay, however, shifts from values averaging ~25% to values averaging ~32% at 15.4 m (Fig. 4). Sand, on the other hand, demonstrates a strong three-tier decrease in values punctuated by two abrupt changes toward lower values at 17.0 and 15.4 m, respectively (Fig. 4). For comparison, the average sand value for the Holocene Lake Elsinore record from Kirby et al. (2010) is shown on Fig. 4. C_{28} *n*-alkanoic acid δD_{wax} values range from −190 to −120‰ over the interval studied (Fig. 4). In general, the δD_{wax} data show a trend toward less negative values from 19.2 to 12.6 m, with two step-

Table 2
Bulk radiocarbon dates and corrections.

Average depth (cm)	Bulk age (cy BP)	Discrete age (cy BP)	Difference (cy BP)
1747.5	16,963[a]	16,139	825
1823.5	18,577	17,433	1144
2019.5	20,852[a]	20,077	776

Average depth (cm)	Uncorrected bulk age (cy BP)	Corrected bulk age (cy BP)
1397	11,858	10,943
1509	12,806	11,891
1541	13,513	12,598
1619	14,045	13,130

Calculated average reservoir effect = 915 ± 163 cy.
[a] $\delta^{13}C$ corrected age.

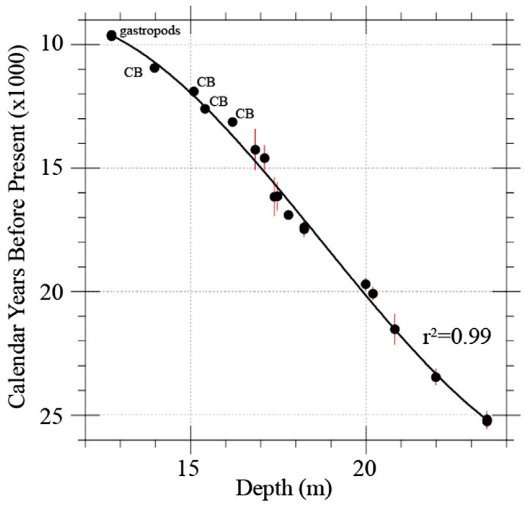

Fig. 3. Age control for LEDC10-1. CB = corrected bulk organic dates (see Table 2 and Results). Red lines represent 2-sigma range.

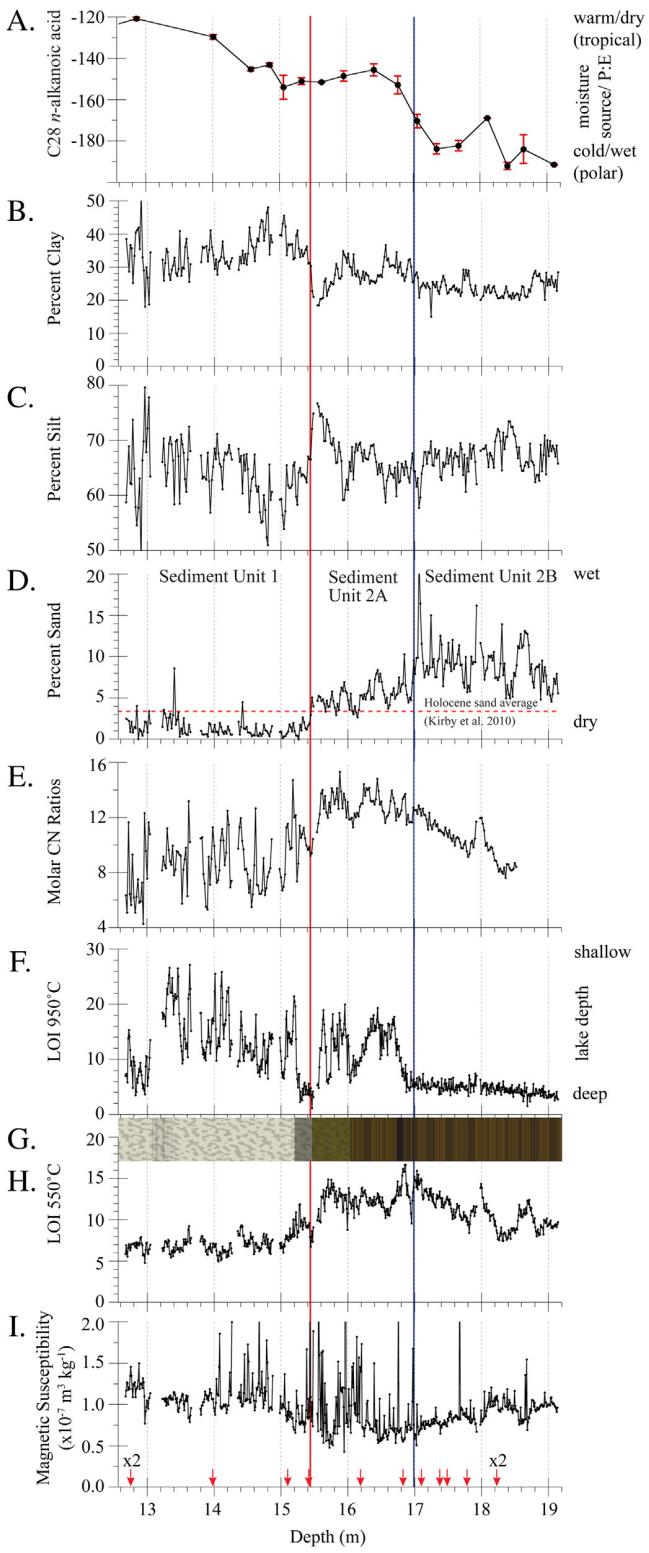

Fig. 4. Sedimentological and geochemical data for LEDC10-1 with stratigraphic column. A) δD_{wax} (‰) (C_{28} *n*-alkanoic acid), B) Percent clay, C) Percent silt, D) Percent sand, E) Molar C:N ratios, F) LOI 950 °C (Percent (%) total carbonate), G) Stratigraphic column, H) LOI 550 °C (Percent (%) total organic matter), I) Magnetic susceptibility. Red arrows represent age control. Vertical red and blue lines represent the statistically defined sediment unit boundaries based on Figs. 5 and 6 (see Discussion).

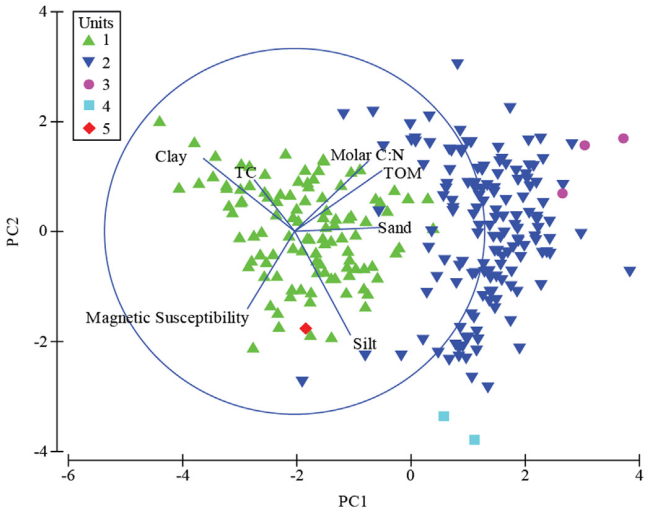

Fig. 5. Principal Component Analysis (PCA) Scatter Plot of the Sample Depths with Measurements for All Proxies. All samples (symbols) and variables (lines) are plotted with respect to the first two eigenvectors (PC1 and PC2) determined from the PCA. The symbols represent the statistical units determined by the Cluster Analysis. TOM = Percent (%) total organic matter (LOI 550 °C); TC = Percent (%) total carbonate (LOI 950 °C).

changes to higher average values starting at approximately 17 and 15 m, respectively.

3.4. Statistical analyses

We identified five cluster groups at a Euclidean distance of 3.7 (cluster data not shown). 3 groups contain only a few outlying samples. Units 1 and 2 are the major units. Unit 1 includes most samples between 12.60 and 15.45 m while Unit 2 includes most of the samples between 15.45 and 18.54 m. Units 1 and 2 are significantly different from one another (ANISOM *R* value of 0.7, $p = 0.001$). Units 1 and 2 are differentiated by PC1 based largely upon sand proportions, accounting for 45.6% of the differences (Fig. 5). We identify sub-units within Unit 2 by running another hierarchical agglomerative clustering analysis. At a Euclidean distance of 3.6, five groups or sub-units clustered out (cluster data not shown). The two main sub-units include Unit 2A and 2B (Fig. 6). Unit 2A contains most samples between 15.45 and 16.96 m while Unit 2B contains most samples between 16.96 and 18.20 m. Units 2A and B are significantly different (ANISOM *R* value 0.715, $p = 0.001$). Units 2A and B, separated by PC1 and PC2, are accounted for by total carbonate (TC) content (Fig. 6) and sand proportions. Together PC1 and 2 account for 66.9% of the variation in the data. As a result, the studied sediment section is divided into Sediment Unit 1, 2A, and 2B based upon their characteristic sand and carbonate contents (Fig. 4).

4. Discussion

4.1. Lake Elsinore proxy interpretations

We have already demonstrated that the sand content in the sediments from Lake Elsinore respond to 20th Century Lake Elsinore lake level, San Jacinto River discharge, and the Pacific Decadal Oscillation Index (Kirby et al., 2010). Wetter conditions (i.e., more run-off) transport more sand to the profundal environment than during drier conditions. High sand content during the most recent glacial and reduced sand content during the Holocene indicate the

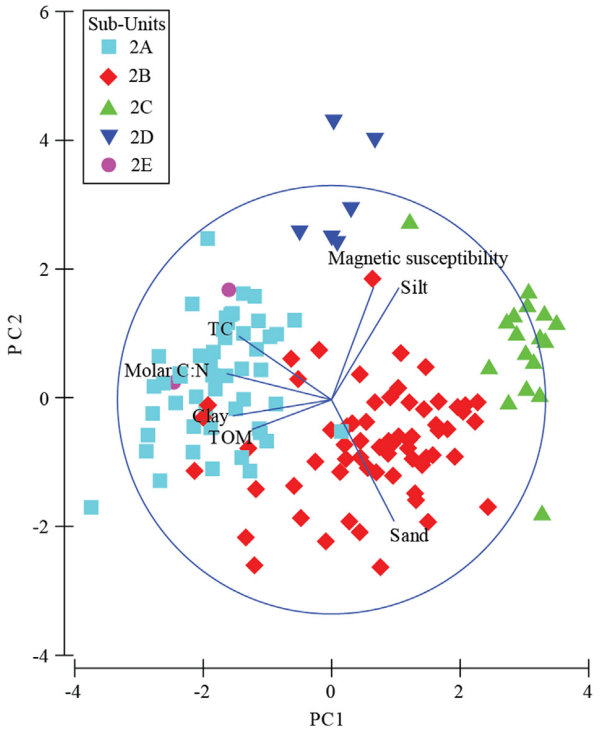

Fig. 6. Principal Component Analysis (PCA) Scatter Plot of the Sample Depths within Statistical Unit 2. All samples (symbols) and variables (lines) are plotted with respect to the first two eigenvectors (PC1 and PC2) determined from the PCA. The symbols represent the statistical sub-units determined by the Cluster Analysis. TOM = Percent (%) total organic matter (LOI 550 °C); TC = Percent (%) total carbonate (LOI 950 °C).

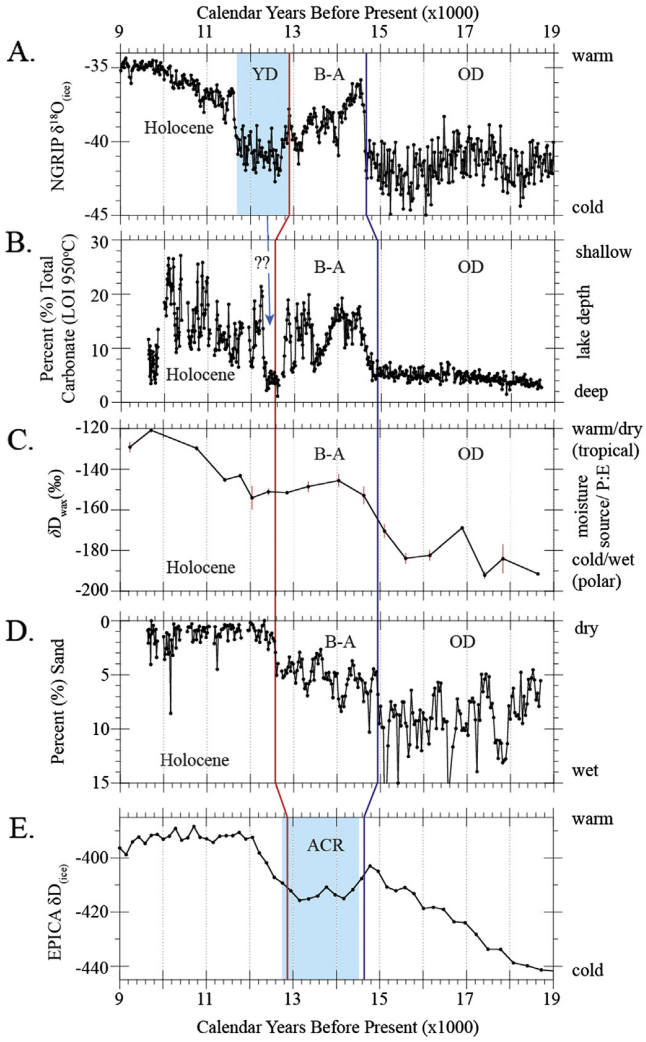

Fig. 7. LEDC10-1 sedimentological and geochemical data compared to ice core data. A) NGRIP oxygen isotope data (Andersen et al., 2006; Rasmussen et al., 2006), B) Percent (%) total carbonate (LOI 950 °C), C) δD_{wax} (‰) (C_{28} *n*-alkanoic acid), D) Percent (%) sand, E) EPICA deuterium isotope data (Augustin et al., 2004). Vertical red and blue lines represent the statistically defined sediment unit boundaries based on Figs. 5 and 6 (see Discussion). Correlation to NGRIP OD to BA and BA to YD boundaries are shown on both A) and E).

expected wet to dry transition consistent with the evidence for replacement of paleo-lakes with playas in the study region (Fig. 4).

We also observe large changes in carbonate content in core LEDC10-1 (Fig. 7). In the modern lake, carbonate precipitates within the epilimnion in response to photosynthetic drawdown of CO_2 (Anderson, 2001), particularly during summer when primary productivity is high and CO_2 drawdown most intense. In addition, higher summer temperatures decrease calcite solubility, enhance evaporation and concentration of the carbonate ions. However, lake depth (a function of climate wetness) may also be related to carbonate preservation, and this may have played a role in the past. Today, Lake Elsinore experiences short-lived, seasonal hypolimnion anoxia. A deeper lake in the past should favor more sustained intervals of hypolimnion anoxia. During anoxia, hypolimnion [CO_2] increases and pH decreases. Together, the latter two limnological changes may act to inhibit the preservation of $CaCO_3$ in the sediment record. Total organic matter and total carbonate are weakly correlated ($r = 0.09$, $n = 1793$) indicating that primary productivity and carbonate production are not tightly coupled in the paleo record (Fig. 4). Total organic matter and C:N are strongly correlated ($r = 0.77$, $n = 265$), which indicates that sediment organic matter in Lake Elsinore is coupled to the contribution of terrestrial organic matter rather than to the contribution of aquatic organic matter (Fig. 4). Carbonate content, therefore, more likely reflects preservation (i.e., hypolimnionic pH/lake depth) than summer epilimnic temperature (i.e., primary productivity).

The hydrogen isotopic composition of plant leaf waxes preserved in sediments has been shown to be a valuable archive of past hydrological change (e.g., Schefusz et al., 2011). The δD_{wax} of plants has been shown to dominantly record the δD of precipitation both globally (Sachse et al., 2012) and locally in southern California (Feakins and Sessions, 2010). We focus on the C_{28} *n*-alkanoic acid, which is both abundant and most likely derived from terrestrial leaf waxes (Kusch et al., 2010). Locally plant leaf waxes have recorded small amplitude shifts (25‰) across 1.4 ka in the Santa Barbara Basin (Li et al., 2009). Here we identify much larger swings (up to 70‰) associated with the larger hydrological reorganizations expected for the deglacial.

The 70‰ variations in δD_{wax} between 19 and 9 ka BP may be related to the isotopic composition of paleoprecipitation with an appropriate fractionation factor between precipitation and leaf wax hydrogen isotopic composition. An appropriate fractionation $\varepsilon_{wax/p}$ is likely between −66 and −100‰. The larger fractionation of −100‰ is based on a study (Hou et al., 2008) of *n*-alkanoic acids in lake coretops in a transect across the southern United States (AZ, NM, TX). The smaller fractionation is based on the local plant based survey of leaf wax *n*-alkanes where fractionations averaged −91‰ (Feakins and Sessions, 2010) adjusted by an expected +25 ± 16‰ based on the offset between alkanes and alkanoic acids reported for

a small sample set (Chikaraishi and Naraoka, 2007). The smaller fractionation (−66‰) appears to generate the most reasonable δD_p values; however, we present the unconverted data because of the uncertainty in the appropriate epsilon to apply without further modern calibration and vegetation change information, which we hope to obtain with future pollen analyses. It is well-known, however, that δD_p is the dominant influence on δD_{wax} (Sachse et al., 2012) and therefore we can interpret the relative changes in δD_{wax} in terms of precipitation. Based on modern observations, North Pacific moisture sources produce rainfall with a lower D/H isotopic composition, whereas subtropical and tropical Pacific, Gulf of Mexico and California sources result in rainfall with a higher D/H isotopic composition (Friedman et al., 2002a). Changes in temperature associated with North Pacific versus subtropical sources are likely to compound these source changes, as colder temperatures of condensation would drive toward more negative values (Dansgaard, 1964; Bowen et al., 2011). In this subtropical coastal context, wetter conditions are expected to drive precipitation toward more negative values and drier conditions to more positive values (the amount effect) (Dansgaard, 1964; Lee and Fung, 2008). Therefore we interpret negative shifts over the Lateglacial as reflecting more northerly, colder and wetter conditions (or wetter conditions) and positive shifts as more southerly, warmer and drier conditions.

4.2. The Lake Elsinore deglacial record

The Lake Elsinore δD_{wax} data is interpreted to reflect a gradual change in the source of winter precipitation from the most recent glacial into the Holocene (Fig. 7). This change toward less negative δD_{wax} values indicates a shift from a dominantly North Pacific winter source during the OD to a more subtropical or tropical winter source in the BA and Holocene.

Sand content indicates a drying trend from the most recent glacial into the Holocene (Fig. 7). Sand content is highest during the OD, decreases during the BA, and further decreases at the start of the YD. This deglacial decline in run-off is consistent with the δD_{wax} evidence for a decrease in the frequency of North Pacific derived winter storms reaching Lake Elsinore's drainage basin leading to the more arid precipitation regime of the Holocene (Fig. 7).

Like both the δD_{wax} and sand data, carbonate content also shifts substantially across the most recent deglacial (Fig. 7). Carbonate is low to absent during the OD, rises to higher and somewhat stable values during the BA, and becomes highly variable by the Holocene. Interpreted as a proxy for epilimnion summer temperature and/or water depth (via inferred hypolimnion anoxia), the carbonate record is concluded to reflect a cold, deep glacial lake evolving into a warm, shallow (possibly fluctuating) Holocene lake, consistent with the δD_{wax} and sand proxies. Together, the multiple proxies indicate a deglacial transition from a cold, wet glacial environment to a warm, drier Holocene environment.

In addition, the sand data demonstrate step changes in the precipitation regime at the transition into and out of the BA. The abruptness of this change is less apparent in the δD_{wax}, perhaps as a result of lower sampling resolution and/or leaf wax resident time in the catchment basin. Notably absent from all of the Lake Elsinore proxies, expect perhaps for the total carbonate, is a distinct hydroclimatic shift between the YD and the Holocene (Fig. 7).

4.3. Regional comparisons

Although we focus on the three sites with the greatest continuity, sample resolution, and age control (Lake Elsinore (CA), Cave of Bells (AZ), and Fort Stanton (NM)), we consider also eight additional sites across the region, which provide a millennial-scale view of paleohydrologic change across the region during the most recent deglacial (Figs. 1 and 8). All the selected sites and proxies record a predominantly hydrologic signal, with the exception of the Santa Barbara Basin *Pinus* pollen and the San Bernardino Mountain glacial extent evidence, which also contain temperature responses (Heusser and Sirocko, 1997; Owen et al., 2003). For each comparison site, however, we focus on the hydroclimatic implications. At each site, we have converted the original radiocarbon dates to calendar years before present to facilitate comparison. We direct the reader to the referenced primary sources for original dating information. Three sites have limited age control: Babicora Basin (Metcalfe et al., 1997; Ortega-Ramírez et al., 1998; Metcalfe et al., 2002; Roy et al., 2012a, 2012b), Paleo-lake San Felipe (Ortega Guerrero et al., 1999; Lozano-Garcia et al., 2002; Roy et al., 2010), and Lake Mojave (Wells et al., 2003) (Figs. 1 and 8); yet, they are included because they fill a spatial gap in coverage.

4.3.1. The Oldest Dryas (19–14.7 ka BP)

In the southwest, the OD is characterized by a climate wetter than today based on the evidence recorded at each of the 11 sites (Figs. 1 and 8). Lake Mojave is reported to change from an intermittent to a permanent lake indicating substantial run-off from the San Bernardino Mountains (Wells et al., 2003). Nearby the Valley Springs site indicates an elevated water-table (Pigati et al., 2011). In northwestern Mexico, paleo-lake San Felipe indicates wet conditions as do groundwater discharge deposits from San Pedro Valley Springs in Arizona (Ortega Guerrero et al., 1999; Lozano-Garcia et al., 2002; Pigati et al., 2009; Roy et al., 2010). The Estancia Basin in New Mexico had high lake levels during the OD except for a 1000-year lowstand centered on 17.5 ka BP (Allen and Anderson, 2000; Anderson et al., 2002). Finally, lake sediments from Babicora Basin in northcentral Mexico indicate probable wetter-than-modern conditions during the OD (Metcalfe et al., 1997; Ortega-Ramírez et al., 1998; Metcalfe et al., 2002; Roy et al., 2012a, 2012b). *Pinus* pollen from a marine core offshore, although variable, is prevalent along the coastal southwest US during the OD indicating wet and/or cold conditions (Heusser and Sirocko, 1997). Glaciers advanced significantly, and perhaps twice, in the San Bernardino Mountains of Southern California during the OD indicating greater winter snowfall (~150% of modern) and lower summer temperatures (Owen et al., 2003). In summary, the southwest is found to be wetter during the OD than the Holocene; although, different amplitude hydrologic variability during the OD is recorded at various sites.

A comparison of the three key sites – Lake Elsinore, Cave of Bells, and Fort Stanton – indicates that the OD was relatively wet across the study region. These sites span the longitudinal breadth of the study region over a narrow latitudinal window, 31.5–33.5°N (Fig. 1). At Lake Elsinore, δD_{wax} values of −190‰ are consistent with more winter precipitation from North Pacific moisture sources, likely linked to a southward displaced polar front jet stream. Increased sand content indicates higher run-off into the Elsinore basin suggesting more frequent and/or larger magnitude winter storms across the Lake Elsinore drainage basin. The Cave of Bells speleothem in Arizona indicates lower, and remarkably stable, $\delta^{18}O_{calcite}$ values interpreted as wetter winter conditions associated with a southerly depressed polar front jet stream and its associated storm tracks (Wagner et al., 2010). The Fort Stanton speleothem from New Mexico indicates lower but highly variable $\delta^{18}O_{calcite}$ values (Asmerom et al., 2010). Unlike the Cave of Bells record, precipitation over Fort Stanton during the OD was much more variable, possibly reflecting a more vigorous monsoonal contribution linked to its eastern location, elevation and concomitant orographic effect on precipitation (Fig. 1). The termination of the OD is abrupt, except for the δD_{wax} data (for reasons mentioned previously), and regionally synchronous. The timing of this transition corresponds to the end of the OD in Greenland (Fig. 7).

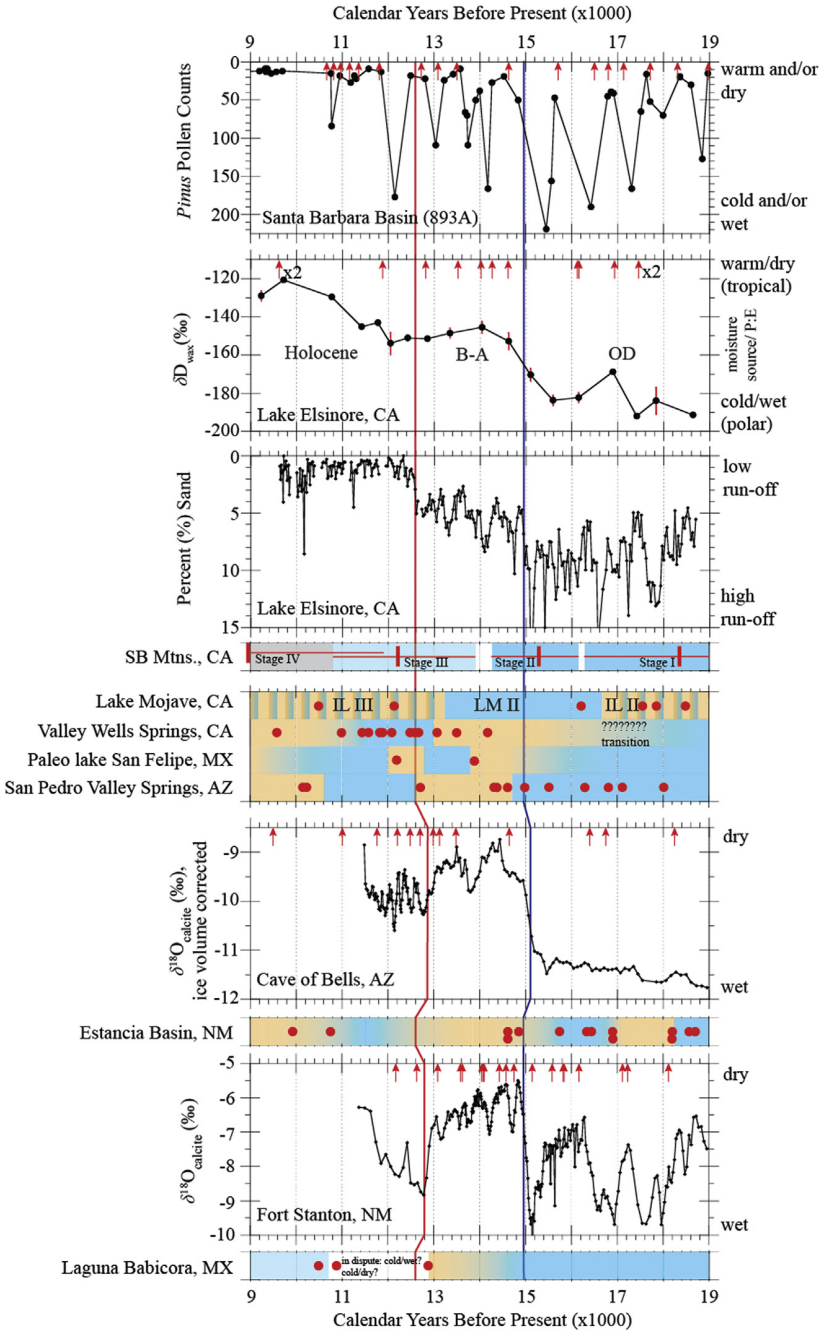

Fig. 8. Study site comparisons. Note that the up direction on all *y*-axes represents dry or warm conditions. Oranges = dry; Blues = wet. Red dots = age control. Red arrows = age control. The range of cosmogenic ages for the San Bernardino Mountains (SB Mtns.) glaciation are shown with a horizontal red line with the average age shown by a short vertical red line. Vertical blue line and red line represent the boundary between Sediment Unit 2B and 2A and Sediment Unit 2A and 1 for Lake Elsinore (see Discussion). Inferred correlations to other sites are shown. See text for site details. IL = Intermittent Lake, LM = Lake Mojave (after Wells et al., 2003).

4.3.2. The BØlling–AllerØd (14.7–12.9 ka BP)

In the southwest, the BA represents a shift to drier conditions following the wet OD (Fig. 8). For Lake Elsinore, the positive change in δD_{wax} values indicates a shift to a lower latitude winter moisture source than during the OD. Run-off into the Elsinore basin is reduced during the BA based on lower sand content, presumably reflecting either less frequent or smaller magnitude winter storms across the Lake Elsinore drainage basin. Lake Mojave becomes an intermittent lake during the late stages of the BA (Wells et al., 2003). Like Elsinore, the Mojave lakes are at the western edge of the study region and fully within the winter-dominated precipitation regime of the headwater San Bernardino Mountain source (Enzel and Wells, 1997). The mismatch between a shift toward drier conditions during the BA at Lake Elsinore and an early BA large sustained lake in the middle of Mojave at the same time is perplexing although not without explanation. A lack of dates between 12.1 and 16.2 ka BP from the Lake Mojave site (Wells et al., 2003) makes it not possible to assign a precise age to the Mojave transitions (Fig. 8). The Valley Springs water-table record indicates a shift toward drier conditions characterized by lowered water-table elevations (Pigati et al., 2011);

however, it is unclear when between 19 and 14.2 ka BP the water table levels fell. From northwestern Mexico, sediment data from Paleo-lake San Felipe indicate a shift toward drier conditions during the BA with a return to wet conditions during the latter half of the BA. Again, limited age control warrants a conservative interpretation of the timing for change (Ortega Guerrero et al., 1999; Lozano-Garcia et al., 2002; Roy et al., 2010). The well-dated San Pedro Valley Spring site indicates a shift toward drier conditions at the beginning of the BA through to the beginning of the YD transition (Pigati et al., 2009). The Cave of Bells speleothem record from Arizona indicates a rapid shift to higher $\delta^{18}O_{calcite}$ during the BA. This change is inferred to represent drier winter conditions caused by a northerly shifted polar front jet stream and its associated storm tracks (Wagner et al., 2010). Estancia Basin in New Mexico was characterized by generally low lake levels during the BA. However, a lack of dates between 14.6 and 10.8 cal ka BP make it difficult to assess the timing (Allen and Anderson, 2000; Anderson et al., 2002). The Fort Stanton, NM speleothem record indicates an abrupt shift to higher $\delta^{18}O_{calcite}$ during the BA (Asmerom et al., 2010). This shift is interpreted to reflect a change to drier winter conditions for reasons similar to Wagner et al. (2010). Finally, lake sediments from Babicora Basin in northcentral Mexico indicate drier conditions during the BA; however, the timing is uncertain (Metcalfe et al., 1997; Ortega-Ramírez et al., 1998; Metcalfe et al., 2002; Roy et al., 2012a). The *Pinus* pollen in a marine core offshore shows a change to less wet and/or less cold conditions during the BA than during the OD (Heusser and Sirocko, 1997). Considering the large age ranges associated with cosmogenic dating, it is arguable that glaciers in the San Bernardino Mountains retreated during the BA indicating less winter snowfall and higher summer temperatures (Owen et al., 2003).

In all, the BA is drier generally than the preceding OD across the study region (Fig. 8). A comparison of our 3 key sites indicates that the transition into and out of the BA was abrupt and that the timing is consistent with the transitions observed in Greenland (Fig. 7). Because Lake Elsinore records winter-only hydrologic variability, we argue that the region-wide drying reflects a decrease in regional winter precipitation (Fig. 8).

4.3.3. The Younger Dryas (12.9–11.7 ka BP)

A hydroclimatic transition between the dry BA into a different climatic state at the start of the YD (12.9 ka BP) is apparent in some, but importantly, not all records (Figs. 1 and 8). At Lake Elsinore, the δD_{wax} data indicate no significant change in moisture source at this time; δD_{wax} values only increase after 12 ka BP (more southerly and/or warmer moisture source). In contrast, in the same core sand content drops abruptly to low and stable levels at the start of the YD through the Holocene, suggesting a rapid decrease in run-off associated with fewer/weaker winter storms starting at 12.6 ka BP (Kirby et al., 2010). If both isotopic and sand proxies are to be interpreted at face value this would suggest a decrease in precipitation amount before a shift in the storm track. Alternatively, the offset may be evidence of a 600-year lag in the average age of the leaf wax residence time in the catchment, perhaps with residence time abruptly increasing with a dry shift, as sediment transport declines rapidly. Carbonate content also decreases abruptly at the same time as the sand (Fig. 8), but with only a 300-year persistence perhaps caused by cooling of the spring/summer epilimnion. Both the *Pinus* and glaciological evidence also support a coastal cooling (Heusser and Sirocko, 1997; Owen et al., 2003). The glacial evidence, however, for a small advance from the San Bernardino Mountains is poorly constrained to within 10.8–13.9 cal ka BP (Owen et al., 2003).

In the Sierra Nevada Mountains of California, there is no evidence for a glacial advance during the YD (Clark and Gillespie, 1997; James et al., 2002; Phillips et al., 2009; Rood et al., 2011). Owens Lake, which drains a large part of the eastern Sierra Nevadas, is characterized by a major lowstand during the YD indicating a decrease in run-off (Bacon et al., 2006). The nature, however, of hydroclimatic changes during the YD have been debated in other records around California. In the east-central Sierra Nevada Mountains, MacDonald et al. (2008) find evidence for lake water cooling during the YD. From the same site, they infer a wet early YD followed by a dry late YD. From the western slope of central Sierra Nevadas, a speleothem record points to a prolonged YD response with colder and variably wet conditions (Oster et al., 2009).

From Lake Mojave, there is no clear YD signal (Wells et al., 2003); although, the lake became more intermittent some time between 13.3 and 9 ka BP. Nearby Valley Springs shows a return to wet conditions 400 years before the start of the YD (Pigati et al., 2011). Thereafter, conditions deteriorated to the modern dry Holocene environment by 11 ka BP (Pigati et al., 2011). Sediment data from Paleo-lake San Felipe in northwestern Mexico indicate a dry YD followed by a return to wet conditions until ~10 ka BP (Ortega Guerrero et al., 1999; Lozano-Garcia et al., 2002; Roy et al., 2010). Groundwater discharge deposits from San Pedro Valley Springs in Arizona indicate a return to wet conditions at the beginning of the YD followed by dry conditions at 10.6 ka BP (Pigati et al., 2009). The beginning of the YD in Estancia Basin is not well constrained by dates; however, it appears that lake level rises modestly during the YD and lowers to Holocene levels by 11 ka BP (Allen and Anderson, 2000; Anderson et al., 2002). Finally, lake sediments from Babicora Basin in northcentral Mexico have yielded contrasting wet/dry interpretations for the YD (Metcalfe et al., 1997; Ortega-Ramírez et al., 1998; Metcalfe et al., 2002). However, recently improved dating indicates that the YD was likely dry at Babicora Basin (Roy et al., 2012a, 2012b).

A comparison of the three key sites indicates that the transition from the dry BA into the YD was abrupt and regionally synchronous; however, the phase of hydrologic change varied between Lake Elsinore (drier than the BA) and the eastern and more inland sites (wetter than the BA). Arizona's Cave of Bells speleothem record shows a small shift to lower average $\delta^{18}O_{calcite}$ values at the start of the YD (Wagner et al., 2010). This shift, however, is less than 0.7‰, which could represent a small temperature change (~2.8 °C) during calcite precipitation with little to no modification of moisture source. A single higher $\delta^{18}O_{calcite}$ value at 11.4 ka BP indicates the probable beginning of the Holocene. The Fort Stanton speleothem record in New Mexico transitions to lower $\delta^{18}O_{calcite}$ values at the beginning of the YD and returns to higher $\delta^{18}O_{calcite}$ values by 11.7 ka BP (Asmerom et al., 2010). A single data point at Cave of Bells and only three data points at Fort Stanton suggest that a climatic perturbation occurred possibly at the end of the YD. There is no apparent termination of the dry event at the Elsinore site as the beginning of the dry YD also marked the beginning of the dry Holocene. Because the winter storms that affect Lake Elsinore should also impact the interior southwest sites, less winter precipitation across Lake Elsinore should also mean less winter precipitation across the entire study region as inferred during the OD and BA. The return to low $\delta^{18}O_{calcite}$ values, however, suggests that winter precipitation likely increased over the interior southwest sites. Perhaps, as an alternative to changing winter moisture, lower temperatures (i.e., less evaporation) coupled with near modern (or enhanced) monsoonal precipitation provided the necessary moisture to create a positive annual hydrologic budget in sites east of Elsinore (Holmgren et al., 2011). There is some evidence that cooler SSTs in the Gulf of Mexico during the latter YD (Flower et al., 2004) may have promoted an enhanced NAM circulation (Maasch and Oglesby, 1990). Is it plausible that this cold Gulf – stronger monsoon scenario, coupled with colder land temperatures, caused the wet YD signal at the interior southwest study site locations. At

this point, the best we can conclude is that the YD was colder across the region than the preceding BA. In addition, net available moisture increased likely east of Lake Elsinore. If winter precipitation is responsible for this increased available moisture, it requires a pattern of winter atmospheric circulation that maintains the dry coastal southwest as observed at Lake Elsinore.

4.4. Dynamical causes of the Oldest Dryas hydroclimatic regime

The unimodal winter precipitation regime at Lake Elsinore provides an opportunity to explore changes in the westerly Pacific sourced moisture separate from changes in the NAM that can confound paleohydrologic interpretations at sites further east. All proxies from Elsinore indicate a wet OD. The δD_{wax} data represent the first opportunity to fingerprint the source of winter moisture to Elsinore during the Lateglacial to Holocene transition, and it allows a direct comparison with the isotopic evidence further east (but with a factor of 8 adjustment between the δD and $\delta^{18}O$ mass dependent fractionations). The leaf wax data from Elsinore show a negative shift of 70‰ relative to the Holocene and strongly suggest that the main source of winter precipitation during the OD was from higher latitude, North Pacific sources and at colder temperatures of condensation than today (Dansgaard, 1964; Friedman et al., 2002a, 2002b; Lee and Fung, 2008). Our interpretation is consistent with the interpretations at Cave of Bells and Fort Stanton based on the oxygen isotopes in speleothem calcite that are likewise recording precipitation changes linked to more northerly winter sources with oxygen isotopic shifts of ~ −11.5 to −9.0‰ (Wagner et al., 2010) and ~ −8.5 to −6.3‰, respectively, between the OD and Holocene.

The negative shift in isotopes in precipitation during the OD recorded at all 3 sites is consistent with a high latitude moisture source. The dipping westerlies hypothesis provides a mechanism for increasing the flux of North Pacific moisture into both the coastal and interior southwest. The presence of the North American ice sheets (both Laurentide and Cordilleran) would have forced the average position of the winter polar front jet stream south and enhanced the strength of the winter season Aleutian Low (see Negrini, 2002 for review). In response to this enhanced low, North Pacific SSTs should have decreased thereby creating a positive feedback to the atmosphere and reinforcing a southward displaced polar front jet stream (Okumura et al., 2009). Consistent with this expectation, cooling in the North Pacific has been reported during the OD (e.g., Lea et al., 2003; Lyle et al., 2010). Thus, the combination of ice sheet extent, strengthened Aleutian Low, and depressed SSTs would have increased the frequency of North Pacific sourced winter storm tracks across the study region.

Our data support a wet OD (19–14.7 ka BP) across the study region. Notably, the Lake Elsinore data contradict the suggestion of a dry coastal California between 17 and 14 ka BP (Lyle et al., 2012). Moreover, we find no isotopic evidence across 3 key sites in the southwest to support their contention that the moisture supply from the North American Monsoon was strengthened during the Lateglacial (Lyle et al., 2012). The isotope data suggest a high latitude North Pacific winter moisture source as well as colder temperatures of condensation during the OD. The data and interpretations are consistent with a southward displacement of the winter polar front jet stream. Therefore, we find that the "dipping westerlies" hypothesis originally proposed by Antevs (1948) is the best explanation for wet conditions in both the coastal and interior southwest during the OD.

4.5. Forcings differ across the interior to coastal southwest

Using the three key sites, we investigate the time period between 19 and 9 ka BP (hereafter the most recent deglacial) (Fig. 9).

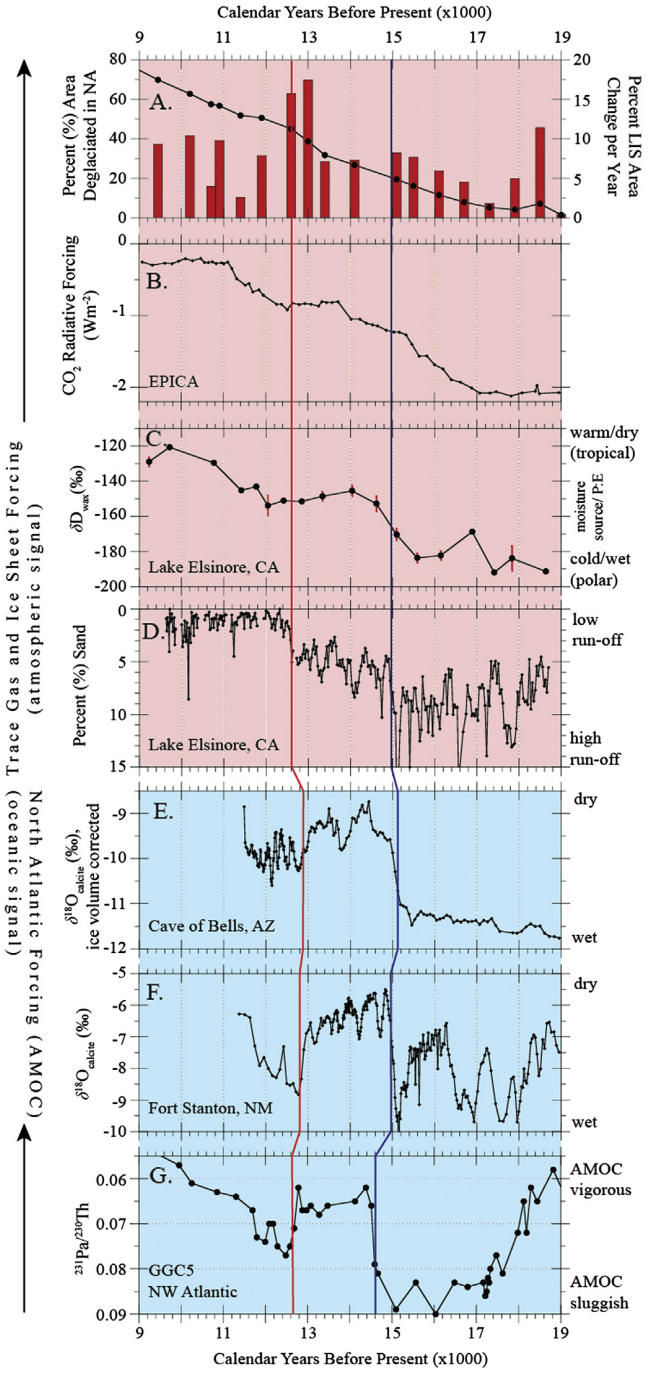

Fig. 9. Regional deglacial sequences and forcings. A) Left *Y*-axis (black dotted line): Percent (%) area deglaciated in North America per year (Dyke, 2004), Right *Y*-axis: Percent (%) Laurentide Ice Sheet (LIS) area change per year (Dyke, 2004), B) CO_2 radiative forcing (Wm^{-2}) per year (Joos and Spahni, 2008), C) δD_{wax} (‰) (C_{28} *n*-alkanoic acid), D) LEDC10-1 percent (%) sand, E) Cave of Bells oxygen isotope data (Wagner et al., 2010), F) Fort Stanton oxygen isotope data (Asmerom et al., 2010), G) $^{231}Pa/^{230}Th$ data (McManus et al., 2004). See text for data details. NA = North America.

The Lake Elsinore record differs markedly from the signals further east at Cave of Bells and Fort Stanton. Lake Elsinore is characterized by a three-step drying sequence (OD to BA to Holocene) separated by two abrupt hydrologic transitions at the OD to BA and the BA to Holocene; there is no apparent YD recorded at Lake Elsinore (Fig. 9). Cave of Bells and Fort Stanton archives track conditions in

Greenland with abrupt transitions between the OD (wet), BA (drier), YD (wet), and Holocene (dry) (Fig. 9). Clearly, different processes are at play between the interior and coastal southwest during the most recent deglacial.

We compare the interior and southwestern US patterns of hydroclimatic change during the most recent deglacial to the principal "modes of deglacial variability" as identified by Clark et al. (2012). Clark et al. (2012) analyzed 166 proxy records for temperature or precipitation and revealed two dominant patterns based upon principal components (PC) analysis. The Global PC1 was found to follow radiative forcing associated with greenhouse gases, particularly CO_2; whereas, the Global PC2 appeared consistent with changes in the AMOC (Fig. 4 from Clark et al., 2012).

Here, we add Lake Elsinore and re-evaluate the forcing of deglacial hydroclimates across the study region in comparison to Clark et al. (2012) Global PC1 and PC2. For PC1, we use CO_2 radiative forcing data from Joos and Spahni (2008) (Fig. 9). We include also the deglaciated area of North America (Dyke, 2004) as a measure of ice sheet extent (Fig. 9). For PC2 we use the North Atlantic $^{231}Pa/^{230}Th$ record as a proxy for AMOC variability (Fig. 9; McManus et al., 2004). We find that the coastal southwest site tracks the Global PC1 deglacial greenhouse gas radiative forcing curve as well as ice extent (Fig. 9) (Clark et al., 2012). The δD_{wax} data lags slightly the CO_2 radiative forcing curve (Fig. 9); however, this lag may reflect a leaf wax residence time issue and/or imprecision implicit in the smoothed nature of the chronology curve in the corresponding range of depth in the Elsinore core (Fig. 3). The long term increase in δD_{wax} data from the glacial into the Holocene is explained best by the 'dipping westerlies' hypothesis. In this scenario, the polar front migrated north and diminished the contribution of North Pacific winter moisture across our study region as greenhouse gases warmed the atmosphere and the continental ice sheets retreated. Mechanistic evidence for a change in the frequency of North Pacific winter cyclogenesis and storm intensity during the most recent glacial has been provided by climate model experiments (e.g., Unterman et al., 2011). They found enhanced winter cyclogenesis and storm intensity in the North Pacific in response to the presence of the North American ice sheets.

Eastward, both Cave of Bells and Fort Stanton (both used in the Clark et al., 2012 analysis) follow the North Atlantic pattern of AMOC variability (Fig. 9). The comparison of records indicates that during reduced AMOC intervals, when N Atlantic SSTs decrease, the amount of precipitation in the interior southwest increases. This is consistent with evidence from the instrumental record (1951–2003 A.D.) that the amount of winter precipitation in the interior southwest US and northern Mexico, is negatively correlated to North Atlantic SSTs (Wagner et al., 2010). Extending this instrumental period relationship into the past, Wagner et al. (2010) cite modeling results to show that a reduction in AMOC strengthens the Aleutian Low and leads to more frequent winter storms across the southwest US (Zhang and Delworth, 2007; Okumura et al., 2009). This mechanism linking the N Atlantic and the southwest US hydroclimatology works for the wet OD and the dry BA; however, the discordance between the 3 sites during the YD requires a mechanism that dries the coastal southwest while wetting the interior southwest. As previously discussed, this mechanism may be related to changes in the contribution of the NAM during the cold YD interval. While changes in the strength of AMOC are more important in the interior southwest, it is important to note that the AMOC does appear to exert a secondary forcing on the Elsinore record, perhaps explaining the abruptness of the transitions in hydroclimate recorded into and out of the BA (Fig. 9).

Our analysis of the most recent deglacial leads us to suggest that the future response to greenhouse gas radiative forcing may not be uniform across the study region. Most predictive climate models implicitly include the coastal southwest as a part of the larger interior southwest (e.g., Seager et al., 2007; Barnett et al., 2008; Dominguez et al., 2012). Our paleoclimatic data suggest the need for a more nuanced consideration of the climatic response that differentiates the coastal versus interior southwest.

5. Summary

We present a new record of hydroclimatic change in the coastal southwestern United States based upon a multi-proxy reconstruction from Lake Elsinore, California spanning 19–9 ka BP. We evaluate the regional climatic significance of this archive in the context of eleven other paleoclimatic reconstructions across the coastal and interior southwestern United States, including northwest Mexico. Three key sites (Lake Elsinore, Cave of Bells, and Fort Stanton) demonstrate that the transitions into and out of the BA were abrupt and synchronous. Region-wide the OD (19–15 ka BP) was wet and the BA (~15–12.7 ka BP) was dry. In contrast, the multi-site evidence indicates that the climate during the YD (~12.7–11.6 ka BP) was variable spatially; coastal sites were dry and interior sites were wet. Given the regional coherence and the evidence particularly from Lake Elsinore, we infer that North Pacific winter season moisture sources account for the OD and BA regime shifts. The opposite response during the YD between the coastal and interior southwest sites is attributed to probable changes in the contribution of NAM moisture to the interior sites and less likely a result of enhanced winter precipitation. The overall structure of the most recent deglacial varies from the coast to the interior southwest and suggests different regional responses to climatic forcings. The coastal site, Elsinore, generally traces radiative forcing from changing greenhouse gas concentrations as well as the retreat of continental ice sheets. The interior southwest sites generally mirror AMOC variability indicating a teleconnection to the N Atlantic. The long term deglacial drying pattern inferred from sand content in Lake Elsinore is complimented by δD_{wax} evidence, which indicates a changing winter moisture sources from North Pacific to subtropical Pacific from the glacial to Holocene, respectively. In conclusion the evidence from Lake Elsinore is consistent with the average position of the winter-season polar front being south of its modern position during the Last Glacial, with the 'dipping westerlies' bringing moisture from high latitude sources into the coastal and interior southwest.

Acknowledgments

Thanks to: Mr. Pat Kilroy (lake manager), the City of Lake Elsinore, John Gregg and Gregg Drilling and Testing, Inc., Joe Holbrook, M.F.A. and the CSUF School of Theatre and Dance for opening the cores; M. Rincon at USC for laboratory assistance. Funding was provided by American Chemical Society – Petroleum Research Grant #48187-B8 to MEK, U.S. National Science Foundation Grants #0318511, 0731843, and 1203549 to MEK and #1203549 to SF. The authors thank Drs. Ingrid Hendy and Linda Heusser for discussions and for access to the pollen data from Santa Barbara Basin. MEK dedicates this paper to Dr. Eugene Domack for giving me my start.

References

Adams, D.K., Comrie, A.C., 1997. The North American monsoon. Bulletin of the American Meteorological Society 78, 2197–2213.

Allen, B.D., Anderson, R.Y., 2000. A continuous, high-resolution record of late Pleistocene climate variability from the Estancia basin, New Mexico. Geological Society of America Bulletin 112, 1444–1458.

Andersen, K.K., Svensson, A., Johnsen, S.J., Rasmussen, S.O., Bigler, M., Röthlisberger, R., Ruth, U., Siggaard-Andersen, M.-L., Peder Steffensen, J., Dahl-Jensen, D., Vinther, B.M., Clausen, H.B., 2006. The Greenland Ice Core

Chronology 2005, 15–42 ka. Part 1: constructing the time scale. Quaternary Science Reviews 25, 3246–3257.
Anderson, M.A., 2001. Internal Loading and Nutrient Cycling in Lake Elsinore. Santa Ana Regional Water Quality Control Board, Lake Elsinore, p. 52.
Anderson, R.Y., Allen, B.D., Menking, K.M., 2002. Geomorphic expression of abrupt climate change in Southwestern North America at the glacial termination. Quaternary Research 57, 371–381.
Antevs, E., 1948. Climatic Changes and Pre-White Man. In: The Great Basin, with Emphasis on Glacial and Postglacial Times, vol. 38. University of Utah Bulletin, pp. 166–191.
Asmerom, Y., Polyak, V.J., Burns, S.J., 2010. Variable winter moisture in the southwestern United States linked to rapid glacial climate shifts. Nature Geoscience 3, 114–117.
Augustin, L., Barbante, C., Barnes, P.R., Barnola, J.M., Bigler, M., Castellano, E., Cattani, O., Chappellaz, J., Dahl-Jensen, D., Delmonte, B., Dreyfus, G., Durand, G., Falourd, S., Fischer, H., Fluckiger, J., Hansson, M.E., Huybrechts, P., Jugie, G., Johnsen, S.J., Jouzel, J., Kaufmann, P., Kipfstuhl, J., Lambert, F., Lipenkov, V.Y., Littot, G.C., Longinelli, A., Lorrain, R., Maggi, V., Masson-Delmotte, V., Miller, H., Mulvaney, R., Oerlemans, J., Oerter, H., Orombelli, G., Parrenin, F., Peel, D.A., Petit, J.R., Raynaud, D., Ritz, C., Ruth, U., Schwander, J., Siegenthaler, U., Souchez, R., Stauffer, B., Steffensen, J.P., Stenni, B., Stocker, T.F., Tabacco, I.E., Udisti, R., Van De Wal, R.S., Van Den Broeke, M., Weiss, J., Wilhelms, F., Winther, J.G., Wolff, E.W., Zucchelli, M., 2004. Eight glacial cycles from an Antarctic ice core. Nature 429, 623–628.
Bacon, S.N., Burke, R.M., Pezzopane, S.K., Jayko, A.S., 2006. Last Glacial maximum and Holocene lake levels of Owens Lake, eastern California, USA. Quaternary Science Reviews 25, 1264–1282.
Barnett, T.P., Pierce, D.W., Hidalgo, H.G., Bonfils, C., Santer, B.D., Das, T., Bala, G., Wood, A.W., Nozawa, T., Mirin, A.A., Cayan, D.R., Dettinger, M.D., 2008. Human-induced changes in the hydrology of the western United States. Science 319, 1080–1083.
Bartlein, P.J., Edwards, M.E., Mock, C.J., Thompson, R.S., Webb, R.S., Webb III, T., Whitlock, C., Anderson, K.H., Anderson, P.M., 1998. Paleoclimate simulations for North America over the past 21,000 years: features of the simulated climate and comparisons with paleoenvironmental data. Quaternary Science Reviews 17, 549–585.
Beuhler, M., 2003. Potential impacts of global warming on water resources in southern California. Water Science and Technology 47, 165–168.
Bowen, G.J., Kennedy, C.D., Liu, Z., Stalker, J., 2011. Water balance model for mean annual hydrogen and oxygen isotope distributions in surface waters of the contiguous United States. Journal of Geophysical Research 116, G04011.
Brodie, C.R., Leng, M.J., Casford, J.S.L., Kendrick, C.P., Lloyd, J.M., Yongqiang, Z., Bird, M.I., 2011. Evidence for bias in C and N concentrations and $\delta^{13}C$ composition of terrestrial and aquatic organic materials due to pre-analysis acid preparation methods. Chemical Geology 282, 67–83.
Burnett, A.W., 1994. Regional-scale troughing over the Southwestern United States: temporal climatology, teleconnections, and climatic impact. Physical Geography 15.
Cayan, D.R., Peterson, D.H., 1989. The influence of North Pacific atmospheric circulation on streamflow in the West in aspects of climate variability in the pacific and the western Americas. In: AGU (Ed.), Geophysical Monograph Series, Washington, pp. 375–397.
Chikaraishi, Y., Naraoka, H., 2007. $\delta^{13}C$ and δD relationships among three n-alkyl compound classes (n-alkanoic acid, n-alkane and n-alkanol) of terrestrial higher plants. Organic Geochemistry 38, 198–215.
Clark, D.H., Gillespie, A.R., 1997. Timing and significance of Late-glacial and Holocene cirque glaciation in the Sierra Nevada, California. Quaternary International 38–39, 21–38.
Clark, P.U., Shakun, J.D., Baker, P.A., Bartlein, P.J., Brewer, S., Brook, E., Carlson, A.E., Cheng, H., Kaufman, D.S., Liu, Z., Marchitto, T.M., Mix, A.C., Morrill, C., Otto-Bliesner, B.L., Pahnke, K., Russell, J.M., Whitlock, C., Adkins, J.F., Blois, J.L., Clark, J., Colman, S.M., Curry, W.B., Flower, B.P., He, F., Johnson, T.C., Lynch-Stieglitz, J., Markgraf, V., McManus, J., Mitrovica, J.X., Moreno, P.I., Williams, J.W., 2012. Global climate evolution during the last deglaciation. Proceedings of the National Academy of Sciences of the United States of America 109, E1134–E1142.
Comrie, A.C., Glenn, E.C., 1998. Principal components-based regionalization of precipitation regimes across the southwest United States and northern Mexico, with an application to monsoon precipitation variability. Climate Research 10, 201–215.
Cook, B.I., Seager, R., Miller, R.L., 2011. On the causes and dynamics of the early twentieth-century north American pluvial*. Journal of Climate 24, 5043–5060.
Dansgaard, W., 1964. Stable isotopes in precipitation. Tellus 16, 436–468.
Dean, W.E., 1974. Determination of carbonate and organic matter in calcareous sedimentary rocks by loss on ignition: comparison with other methods. Journal of Sedimentary Petrology 44, 242–248.
Dettinger, M.D., Ralph, F.M., Das, T., Neiman, P.J., Cayan, D.R., 2011. Atmospheric rivers, floods and the water resources of California. Water 3, 445–478.
Dominguez, F., Rivera, E., Lettenmaier, D.P., Castro, C.L., 2012. Changes in winter precipitation extremes for the western United States under a warmer climate as simulated by regional climate models. Geophysical Research Letters 39, L05803.
Dyke, A.S., 2004. An outline of North American deglaciation with emphasis on central and northern Canada. In: Ehlers, J., Gibbard, P.L. (Eds.), Developments in Quaternary Sciences. Elsevier, pp. 373–424.
Ely, L.L., Enzel, Y., Cayan, D.R., 1994. Anomalous North Pacific atmospheric circulation and large winter floods in the Southwestern United States. Journal of Climate 7, 977–987.
Enzel, Y., Wells, S.G., 1997. Extracting Holocene paleohydrology and paleoclimatology information from modern extreme flood events: an example from southern California. Geomorphology 19, 203–226.
Fantozzi, J.M., 2011. Reconstruction of Hydrologic Variability at Lake Elsinore, California, During the Late-Glacial to Holocene Transition. In: Geological Sciences. California State University, Fullerton, Fullerton, CA, p. 94.
Feakins, S.J., Sessions, A.L., 2010. Controls on the D/H ratios of plant leaf waxes in an arid ecosystem. Geochimica et Cosmochimica Acta 74, 2128–2141.
Flower, B.P., Hastings, D.W., Hill, H.W., Quinn, T.M., 2004. Phasing of deglacial warming and Laurentide Ice Sheet meltwater in the Gulf of Mexico. Geology 32, 597–600.
Friedman, I., Harris, J.M., Smith, G.I., Johnson, C.A., 2002a. Stable isotope composition of waters in the Great Basin, United States 1. Air-mass trajectories. Journal of Geophysical Research 107, 4400.
Friedman, I., Smith, G.I., Gleason, J.D., Warden, A., Harris, J.M., 1992. Stable isotope composition of waters in Southeastern California 1. Modern precipitation. Journal of Geophysical Research 97, 5795–5812.
Friedman, I., Smith, G.I., Johnson, C.A., Moscati, R.J., 2002b. Stable isotope compositions of waters in the Great Basin, United States 2. Modern precipitation. Journal of Geophysical Research D: Atmospheres 107, 15-11–15-21.
Heusser, L., Sirocko, F., 1997. Millennial pulsing of environmental change in southern California from the past 24 k.y: a record of Indo-Pacific ENSO events? Geology 25, 243–246.
Holmgren, C.A., Betancourt, J.L., Rylander, K.A., 2011. Vegetation history along the eastern, desert escarpment of the Sierra San Pedro Mártir, Baja California, Mexico. Quaternary Research 75, 647–657.
Hou, J., D'Andrea, W.J., Huang, Y., 2008. Can sedimentary leaf waxes record D/H ratios of continental precipitation? Field, model, and experimental assessments. Geochimica et Cosmochimica Acta 72, 3503–3517.
Hull, A.G., 1990. Seismotectonics of the Elsinore-Temecula Trough, Elsinore Fault Zone, Southern California. In: Geological Sciences. UC Santa Barbara, Santa Barbara, p. 233.
Hull, A.G., Nicholson, C., 1992. Seismotectonics of the northern Elsinore fault zone, southern California. Bulletin of the Seismological Society of America 82, 800–818.
IPCC, 2007. Climate change 2007. In: Pachauri, R.K., Reisinger, A. (Eds.), Synthesis Report. IPCC, Geneva, p. 104.
James, L.A., Harbor, J., Fabel, D., Dahms, D., Elmore, D., 2002. Late Pleistocene glaciations in the Northwestern Sierra Nevada, California. Quaternary Research 57, 409–419.
Joos, F., Spahni, R., 2008. Rates of change in natural and anthropogenic radiative forcing over the past 20,000 years. Proceedings of the National Academy of Sciences of the United States of America 105, 1425–1430.
Kim, S.-J., Crowley, T., Erickson, D., Govindasamy, B., Duffy, P., Lee, B., 2008. High-resolution climate simulation of the Last Glacial Maximum. Climate Dynamics 31, 1–16.
Kirby, M., Lund, S., Patterson, W., Anderson, M., Bird, B., Ivanovici, L., Monarrez, P., Nielsen, S., 2010. A Holocene record of Pacific Decadal Oscillation (PDO)-related hydrologic variability in Southern California (Lake Elsinore, CA). Journal of Paleolimnology 44, 819–839.
Kirby, M.E., Poulsen, C.J., Lund, S.P., Patterson, W.P., Reidy, L., Hammond, D.E., 2004. Late Holocene lake-level dynamics inferred from magnetic susceptibility and stable oxygen isotope data: Lake Elsinore, Southern California (USA). Journal of Paleolimnology 31, 275–293.
Kirby, M.E., Zimmerman, S.R.H., Patterson, W.P., Rivera, J.J., 2012. A 9170-year record of decadal-to-multi-centennial scale pluvial episodes from the coastal Southwest United States: a role for atmospheric rivers? Quaternary Science Reviews 46, 57–65.
Kusch, S., Rethemeyer, J., Schefuß, E., Mollenhauer, G., 2010. Controls on the age of vascular plant biomarkers in Black Sea sediments. Geochimica et Cosmochimica Acta 74, 7031–7047.
Lawrence, M.B., Avila, L.A., Beven, J.L., Franklin, J.L., Pasch, R.J., Stewart, S.R., 2001. Eastern North Pacific hurricane season of 2000. Monthly Weather Review 129, 3004–3014.
Lea, D.W., Pak, D.K., Peterson, L.C., Hughen, K.A., 2003. Synchroneity of tropical and high-latitude Atlantic temperatures over the Last Glacial termination. Science 301, 1361–1364.
Lee, J.-E., Fung, I., 2008. "Amount effect" of water isotopes and quantitative analysis of post-condensation processes. Hydrological Processes 22, 1–8.
Li, C., Sessions, A.L., Kinnaman, F.S., Valentine, D.L., 2009. Hydrogen-isotopic variability in lipids from Santa Barbara Basin sediments. Geochimica et Cosmochimica Acta 73, 4803–4823.
Lozano-García, M.a.S., Ortega-Guerrero, B., Sosa-Nájera, S., 2002. Mid- to late-Wisconsin pollen record of San Felipe Basin, Baja California. Quaternary Research 58, 84–92.
Lyle, M., Heusser, L., Ravelo, C., Andreasen, D., Olivarez Lyle, A., Diffenbaugh, N., 2010. Pleistocene water cycle and eastern boundary current processes along the California continental margin. Paleoceanography 25, PA4211.
Lyle, M., Heusser, L., Ravelo, C., Yamamoto, M., Barron, J., Diffenbaugh, N.S., Herbert, T., Andreasen, D., 2012. Out of the tropics: the Pacific, Great Basin Lakes, and Late Pleistocene Water Cycle in the Western United States. Science 337, 1629–1633.
Lynch, H.B., 1931. Rainfall and Stream Run-off in Southern California Since 1769. The Metropolitan Water District of Southern California, Los Angeles, p. 31.
Maasch, K.A., Oglesby, R.J., 1990. Meltwater cooling of the Gulf of Mexico: a GCM simulation of climatic conditions at 12 ka. Paleoceanography 5, 977–996.
MacDonald, G.M., Moser, K.A., Bloom, A.M., Porinchu, D.F., Potito, A.P., Wolfe, B.B., Edwards, T.W.D., Petel, A., Orme, A.R., Orme, A.J., 2008. Evidence of temperature

depression and hydrological variations in the eastern Sierra Nevada during the Younger Dryas stade. Quaternary Research 70, 131–140.
McFadden, M.A., Patterson, W.P., Mullins, H.T., Anderson, W.T., 2005. Multi-proxy approach to long- and short-term Holocene climate-change: evidence from eastern Lake Ontario. Journal of Paleolimnology 33, 371–391.
McManus, J.F., Francois, R., Gherardi, J.M., Keigwin, L.D., Brown-Leger, S., 2004. Collapse and rapid resumption of Atlantic meridional circulation linked to deglacial climate changes. Nature 428, 834–837.
Metcalfe, S., Say, A., Black, S., McCulloch, R., O'Hara, S., 2002. Wet conditions during the Last Glaciation in the Chihuahuan Desert, Alta Babicora Basin, Mexico. Quaternary Research 57, 91–101.
Metcalfe, S.E., Bimpson, A., Courtice, A.J., O'Hara, S.L., Taylor, D.M., 1997. Climate change at the monsoon/Westerly boundary in Northern Mexico. Journal of Paleolimnology 17, 155–171.
Negrini, R.M., 2002. Pluvial lake sizes in the Northwestern Great Basin throughout the Quaternary Period. In: Hersler (Ed.), Great Basin Aquatics Systems History. Smithsonian Press, Washington, DC, pp. 11–52.
Neiman, P.J., Ralph, F.M., Wick, G.A., Lundquist, J.D., Dettinger, M.D., 2008. Meteorological characteristics and overland precipitation impacts of atmospheric rivers affecting the West Coast of North America based on eight years of SSM/I satellite observations. Journal of Hydrometeorology 9, 22–47.
Okumura, Y.M., Deser, C., Hu, A., Xie, S.P., Timmermann, A., 2009. North Pacific climate response to freshwater forcing in the subarctic North Atlantic: oceanic and atmospheric pathways. Journal of Climate 22, 1424–1445.
Ortega Guerrero, B., Caballero Miranda, M., Lozano García, S., De la O Villanueva, M., 1999. Palaeoenvironmental Record of the Last 70 000 Yr in San Felipe Basin, Sonora Desert, Mexico: Preliminary Results. Universidad Nacional Autónoma de México, Instituto de Geofísica.
Ortega-Ramírez, J.R., Valiente-Banuet, A., Urrutia-Fucugauchi, J., Mortera-Gutiérrez, C.A., Alvarado-Valdez, G., 1998. Paleoclimatic changes during the Late Pleistocene – Holocene in Laguna Babícora, near the Chihuahuan Desert, México. Canadian Journal of Earth Sciences 35, 1168–1179.
Oster, J.L., MontaÒez, I.P., Sharp, W.D., Cooper, K.M., 2009. Late Pleistocene California droughts during deglaciation and Arctic warming. Earth and Planetary Science Letters 288, 434–443.
Overpeck, J.T., 1996. Warm climate surprises. Science 271, 1820–1821.
Owen, L.A., Finkel, R.C., Minnich, R.A., Perez, A.E., 2003. Extreme southwestern margin of late Quaternary glaciation in North America: timing and controls. Geology 31, 729–732.
Phillips, F.M., Zreda, M., Plummer, M.A., Elmore, D., Clark, D.H., 2009. Glacial geology and chronology of Bishop Creek and vicinity, eastern Sierra Nevada, California. Geological Society of America Bulletin 121, 1013–1033.
Pigati, J.S., Bright, J.E., Shanahan, T.M., Mahan, S.A., 2009. Late Pleistocene paleohydrology near the boundary of the Sonoran and Chihuahuan Deserts, southeastern Arizona, USA. Quaternary Science Reviews 28, 286–300.
Pigati, J.S., Miller, D.M., Bright, J.E., Mahan, S.A., Nekola, J.C., Paces, J.B., 2011. Chronology, sedimentology, and microfauna of groundwater discharge deposits in the central Mojave Desert, Valley Wells, California. Geological Society of America Bulletin 123, 2224–2239.
Pyke, B.N., Kirby, M.E., Scholz, C.A., Cattaneo, P., 2009. Seismic reflection data from Lake Elsinore, Southern CA, reveal a sustained late-Holocene lake lowstand. American Geophysical Union. Eos Transactions. San Francisco, pp. PP11B-1317.
Rasmussen, S.O., Andersen, K.K., Svensson, A.M., Steffensen, J.P., Vinther, B.M., Clausen, H.B., Siggaard-Andersen, M.L., Johnsen, S.J., Larsen, L.B., Dahl-Jensen, D., Bigler, M., Röthlisberger, R., Fischer, H., Goto-Azuma, K., Hansson, M.E., Ruth, U., 2006. A new Greenland ice core chronology for the Last Glacial termination. Journal of Geophysical Research: Atmospheres 111.
Ritchie, E.A., Wood, K.M., Gutzler, D.S., White, S.R., 2011. The influence of eastern Pacific tropical cyclone remnants on the Southwestern United States. Monthly Weather Review 139, 192–210.
Rood, D.H., Burbank, D.W., Finkel, R.C., 2011. Chronology of glaciations in the Sierra Nevada, California, from ^{10}Be surface exposure dating. Quaternary Science Reviews 30, 646–661.
Roy, P.D., Caballero, M., Lozano, R., Ortega, B., Lozano, S., Pi, T., Israde, I., Morton, O., 2010. Geochemical record of Late Quaternary paleoclimate from lacustrine sediments of paleo-lake San Felipe, western Sonora Desert, Mexico. Journal of South American Earth Sciences 29, 586–596.
Roy, P.D., Jonathan, M.P., Pérez-Cruz, L.L., Sánchez-Córdova, M.M., Quiroz-Jiménez, J.D., Romero, F.M., 2012a. A millennial-scale Late Pleistocene–Holocene palaeoclimatic record from the western Chihuahua Desert, Mexico. Boreas 41, 707–718.
Roy, P.D., Quiroz-Jiménez, J.D., Pérez-Cruz, L.L., Lozano-García, S., Metcalfe, S.E., Lozano-Santacruz, R., López-Balbiaux, N., Sánchez-Zavala, J.L., Romero, F.M., 2012b. Late Quaternary paleohydrological conditions in the drylands of northern Mexico: a summer precipitation proxy record of the last 80 cal ka BP. Quaternary Science Reviews (in press). Available online: 23 December 2012.
Sachse, D., Billault, I., Bowen, G.J., Chikaraishi, Y., Dawson, T.E., Feakins, S.J., Freeman, K.H., Magill, C.R., McInerney, F.A., van der Meer, M.T.J., Polissar, P., Robins, R.J., Sachs, J.P., Schmidt, H.-L., Sessions, A.L., White, J.W.C., West, J.B., Kahmen, A., 2012. Molecular Paleohydrology: interpreting the hydrogen-isotopic composition of lipid biomarkers from photosynthesizing organisms. Annual Review of Earth and Planetary Sciences 40, 221–249.
Schefusz, E., Kuhlmann, H., Mollenhauer, G., Prange, M., Patzold, J., 2011. Forcing of wet phases in southeast Africa over the past 17,000 years. Nature 480, 509–512.
Seager, R., Kushnir, Y., Herweijer, C., Naik, N., Velez, J., 2005. Modeling of tropical forcing of persistent droughts and pluvials over Western North America: 1856–2000*. Journal of Climate 18, 4065–4088.
Seager, R., Ting, M., Held, I., Kushnir, Y., Lu, J., Vecchi, G., Huang, H.-P., Harnik, N., Leetmaa, A., Lau, N.-C., Li, C., Velez, J., Naik, N., 2007. Model projections of an imminent transition to a more arid climate in Southwestern North America. Science 316, 1181–1184.
Sessions, A.L., Burgoyne, T.W., Hayes, J.M., 2001. Correction of H3+ contributions in hydrogen isotope ratio monitoring mass spectrometry. Analytical Chemistry 73, 192–199.
Sheppard, P.R., Comrie, A.C., Packin, G.D., Angersbach, K., Hughes, M.K., 2002. The climate of the US Southwest. Climate Research 21, 219–238.
Smith, K., 2011. We are seven billion. Nature Clim. Change 1, 331–335.
Stensrud, D.J., Gall, R.L., Mullen, S.L., Howard, K.W., 1995. Model climatology of the Mexican monsoon. Journal of Climate 8, 1775–1794.
Stuiver, M., Reimer, P.J., Bard, E., Beck, J.W., Burr, G.S., Hughen, K.A., Kromer, B., McCormac, G., Plicht, J.v.d., Spurk, M., 1998. INTCAL98 radiocarbon age calibration, 24,000–0 cal BP. Radiocarbon 40, 1041–1083.
Tchakerian, V.P., Lancaster, N., 2002. Late Quaternary arid/humid cycles in the Mojave Desert and western Great Basin of North America. Quaternary Science Reviews 21, 799–810.
Unterman, M.B., Crowley, T.J., Hodges, K.I., Kim, S.J., Erickson, D.J., 2011. Paleometeorology: high resolution Northern Hemisphere wintertime mid-latitude dynamics during the Last Glacial Maximum. Geophysical Research Letters 38, L23702.
Vaughan, P.R., Thorup, K.M., Rockwell, T.K., 1999. Paleoseismology of the Elsinore fault at Agua Tibia Mountain, southern California. Bulletin of the Seismological Society of America 89, 1447–1457.
Wagner, J.D.M., Cole, J.E., Beck, J.W., Patchett, P.J., Henderson, G.M., Barnett, H.R., 2010. Moisture variability in the southwestern United States linked to abrupt glacial climate change. Nature Geoscience 3, 110–113.
Wells, S.G., Brown, J.B., Enzel, Y., Anderson, R.Y., McFadden, L.D., 2003. Late Quaternary geology and paleohydrology of pluvial Lake Mojave, southern California. In: Enzel, Y., Wells, S.G., Lancaster, N. (Eds.), Paleoenvironments and Paleohydrology of the Mojave and Southern Great Basin Deserts. Geological Society of America, Boulder, CO, pp. 79–115.
Williams, A.E., Rodoni, D.P., 1997. Regional isotope effects and application to hydrologic investigations in southwestern California. Water Resources Research 33, 1721–1729.
Wright, W.E., Long, A., Comrie, A.C., Leavitt, S.W., Cavazos, T., Eastoe, C., 2001. Monsoonal moisture sources revealed using temperature, precipitation, and precipitation stable isotope timeseries. Geophysical Research Letters 28, 787–790.
Zhang, R., Delworth, T.L., 2007. Impact of the Atlantic Multidecadal Oscillation on North Pacific climate variability. Geophysical Research Letters 34, L23708.